REPORT DOCUMENTATION PAGE

Form Approved
OMB NO. 0704-0188

1. AGENCY USE ONLY (Leave Blank)	2. REPORT DATE 12/14/2004	3. REPORT TYPE AND DATES COVERED Final Report: 05/15/2001-09/14/2004

4. TITLE AND SUBTITLE
Study of the formation mechanism of self-assembled quantum dot arrays with a focus on alloying and nucleation control

5. FUNDING NUMBERS
DAAD19-01-1-0532

6. AUTHOR(S)
Ya-Hong Xie, HyungJun Kim, ZuoMing Zhao, Bin Shi, Jian Liu, Oksana Hul'ko

7. PERFORMING ORGANIZATION NAME(S) AND ADDRESS(ES)
University of California Los Angeles
Bos 951595 Los Angeles, CA 90095-1595

8. PERFORMING ORGANIZATION REPORT NUMBER 2004

9. SPONSORING / MONITORING AGENCY NAME(S) AND ADDRESS(ES)
U. S. Army Research Office
P.O. Box 12211
Research Triangle Park, NC 27709-2211

10. SPONSORING / MONITORING AGENCY REPORT NUMBER
42412.1-MS

11. SUPPLEMENTARY NOTES
The views, opinions and/or findings contained in this report are those of the author(s) and should not be construed as an official Department of the Army position, policy or decision, unless so designated by other documentation.

12 a. DISTRIBUTION / AVAILABILITY STATEMENT
Approved for public release; distribution unlimited.

12 b. DISTRIBUTION CODE

13. ABSTRACT (Maximum 200 words)

The objective of the research project is to further the understanding of key materials science with regard to the formation mechanism of semiconductor self assembled quantum dots via epitaxy. During the funding period of 3+ years, we have made significant progress in that direction. We have conducted in depth study on the following specific topics: the importance of alloying during epitaxial growth of SAQDs, the function of buried misfit dislocation in guided self-assembly by epitaxy, key issues pertinent to the growth of III-V on Si (001), and finally, the feasibility of fabricating quantum dot lasers of InAs or GaAs on Si. The importance of alloying was studied using the combination of Ge SAQD on Si in which the critical dot size for pyramid-to-dome transition was shown to increase significantly with increasing intermixing between Ge and Si. Using a buried misfit dislocation network, we have been able to demonstrate 3 distinctively different types of nucleation sites on Si (001). Further more, a properly designed, partially relaxed SiGe buffer layer has been shown to be a valuable vehicle for studying the formation mechanism of Ge SAQDs on Si. One of the applications was to experimentally determine the diffusion constant of Ge on Si and on Sb covered Si. We have also shown that the growth of III-V on Si is via Vomer-Weber mode without a wetting layer. Furthermore, the critical dot size for dislocation of InAs SAQDs on Si is less than 5 nm, making it a fundamental hurdle for fabricating lasers on Si.

14. SUBJECT TERMS
quantum dots, adatom, surface diffusion, activation energy, dislocation, growth mode

15. NUMBER OF PAGES

16. PRICE CODE

17. SECURITY CLASSIFICATION OR REPORT	18. SECURITY CLASSIFICATION ON THIS PAGE	19. SECURITY CLASSIFICATION OF ABSTRACT	20. LIMITATION OF ABSTRACT
UNCLASSIFIED	**UNCLASSIFIED**	**UNCLASSIFIED**	**UL**

Proposal title: Study of the formation mechanism of self-assembled quantum dot arrays with a focus on alloying and nucleation control

ARO Contract #: DAAD19-01-1-0532

Beginning date: 15 May, 2001

ARO technical representative: Dr. John Prater

Abstract

The objective of the research project is to further the understanding of key materials science with regard to the formation mechanism of semiconductor self assembled quantum dots via epitaxy. During the funding period of 3+ years, we have made significant progress in that direction. We have conducted in depth study on the following specific topics: the importance of alloying during epitaxial growth of SAQDs, the function of buried misfit dislocation in guided self-assembly by epitaxy, key issues pertinent to the growth of III-V on Si (001), and finally, the feasibility of fabricating quantum dot lasers of InAs or GaAs on Si. The importance of alloying was studied using the combination of Ge SAQD on Si in which the critical dot size for pyramid-to-dome transition was shown to increase significantly with increasing intermixing between Ge and Si. Using a buried misfit dislocation network, we have been able to demonstrate 3 distinctively different types of nucleation sites on Si (001). Further more, a properly designed, partially relaxed SiGe buffer layer has been shown to be a valuable vehicle for studying the formation mechanism of Ge SAQDs on Si. One of the applications was to experimentally determine the diffusion constant of Ge on Si and on Sb covered Si. We have also shown that the growth of III-V on Si is via Vomer-Weber mode without a wetting layer. Furthermore, the critical dot size for dislocation of InAs SAQDs on Si is less than 5 nm, making it a fundamental hurdle for fabricating lasers on Si. The emphasis of the proposed research program is the understanding of the impact of alloying on the formation mechanism of self-assembled quantum dots (SAQD), and the nucleation control using an undulating strain field.

Our first report covering the period since the starting of this program on May 15, 2001 till December 31, 2002 described our observation and understanding regarding the drastic contrast between the one-step and two-step growth approaches for Ge SAQDs on Si. Our second report for the period from January 1, 2002 till December 31, 2002 described the understanding for the various stages of the nucleation and growth of Ge SAQDs at three different types of sites on the surface and growth condition mapping for InAs SAQDs on Si.

Our second report covered the period from April 1, 2003 till December 31, 2003.The progress includes that: 1) we determined the surface diffusion coefficient (2.53×10^{-7} cm^2/sec) and the activation energy (0.676 ± 0.03 eV) of Ge adatoms on Si(001) in the temperature range from 650 °C to 725 °C. This is achieved by using Ge SAQDs grown on a relaxed SiGe buffer layer with the spacing between dislocations that is much larger than the average surface diffusion length of Ge adatoms at various growth temperatures. The surface diffusion coefficient is determined by the inter-dot spacing (d_i) in the region far away from dislocations. 2) we finished the mapping of the parameter space for the growth. We are able to control InAs SAQDs: density from 10^9 cm^{-2} to 10^{11} cm^{-2}, dot diameter from 9 nm to 30 nm, dot height from 4nm to 15nm and size distribution within 30%. We have also carried out detailed transmission electron microscopy (TEM) study of

individual dots. Based on Morie pattern analysis we have experimentally identified the critical dot size for threading dislocation under different growth conditions. These have made good preparation for laser application. We are starting to understand the physics about dot formation. From both experiments and theoretical calculation, we have proved the Volmer-Weber growth mode for InAs on Si.

Our progress made in the period from January 1, 2004 till September 14, 2004 includes the following: 1) Clear contrast between InAs dots on Si (001) and GaAs quantum dots on Si (001) is observed. InAs dot density is strongly dependent on arsenic beam equivalent pressure (BEP), while GaAs quantum dot density is independent on arsenic BEP. 2) High resolution transmission electron microscopy was used to study dislocation formation in InAs dots. Misfit dislocation formed at very early stage of dot growth, size below 5nm. Both 60^o and 90^o dislocation were observed at the interface. 3) InAs quantum dots on GaAs (001) were also studied. A way to separately control dot density and uniformity is developed. InAs quantum dots with high density and high uniformity on GaAs (001) are grown with two steps, low-temperature dot nucleation and high-temperature dot growth.

Highlight of Research Accomplishment

1. Ge quantum dots on Si (001)

1) **Alloying study**: Our ultimate goal for carrying out this line of study is to understand the dominant factors influencing the SAQD size uniformity. This, combined with the well-known fact of the prominent pyramid-to-dome transition in the Ge/Si system, and the lack of understanding on the transition process, prompted us to take a close look at the alloying between SAQDs and the substrate. The reason for using the Ge/Si system for the study is the availability of a relatively large volume of published literature, and the MBE system. Similar study will be carried out in InAs/GaAs system once the MBE system becomes operational.

   Our experimental approach consists of a very low temperature (~250ºC) growth of Ge wetting layer (~5 Å thick) on Si, followed by raising the substrate temperature to 650ºC to grow Ge dots of various size. The rationale is that the low temperature wetting-layer turns the kinetics of the alloying from a surface process to a bulk process. We expect the activation barrier for alloying between the two cases to differ significantly, with the bulk process being at much lower speed. The potentially poor quality of the wetting layer should be improved during the time when the substrate temperature is raised to 650ºC.

   Fig. 1a & 1b are two AFM images. The only difference between the two samples is that sample b has a low temperature wetting-layer, whereas sample a does not. The improved dot uniformity is clearly visible. For the two-step samples with the low temperature wetting-layer, the pyramid-to-dome transition occurs at a lower Ge coverage than that for a one-step sample (fig. 2). From thermodynamic, it is intuitive to expect that the dome shape, which consists of larger angle facets, should prevail at higher misfit strain. Our result is in principle consistent with that expectation. This is because low temperature wetting-layer growth results in less degree of alloying between Ge and Si, and the effective concentration of Ge in the SAQDs is higher for the two-step samples.

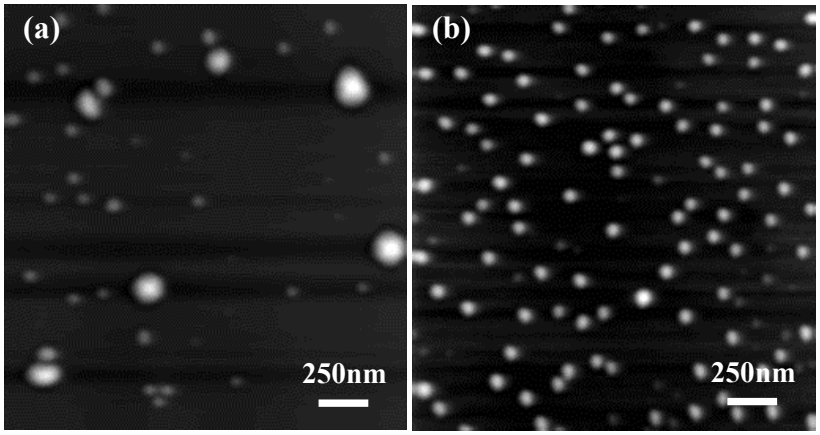

Fig. 1. Two-dimensional 2μm × 2μm AFM topographic images of 7.0Å Ge coverage on Si(001) substrate without a buried misfit dislocation network. a) one-step growth, b) two-step growth.

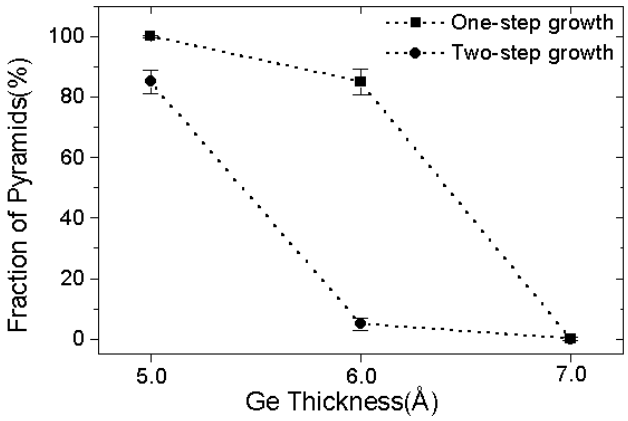

Fig. 2. Variation of the fraction of pyramids in the samples with various Ge coverages grown both by one-step and two-step growths.

To verify this hypothesis, we carried out further experiments to study the detailed shape of SAQDs of Ge grown on partially relaxed SiGe substrates. The substrates are fabricated in such a fashion that the dislocation spacing is larger than the diffusion length of Ge on the surface. As a result, we have two groups of Ge SAQDs. One group of regularly spaced dots that located preferentially over the buried dislocation inter-sections, and one that consists randomly nucleated dots. We used planview TEM to ensure that the regularly spaced dots are indeed located at the precise point where the two slip planes of two intersecting dislocations meet the surface (fig.3). Furthermore, there is a distinct difference between the critical dot size for the pyramid-to-dome transition. The critical size is ~920 Å for dots above dislocations and ~800 Å for randomly nucleated dots. This observation is consistent with the low temperature wetting-layer experiments. The region of the substrate surface over dislocation intersections has larger lattice constant, that in turn leads to a lower misfit strain in the Ge dots, and therefore a larger critical size.

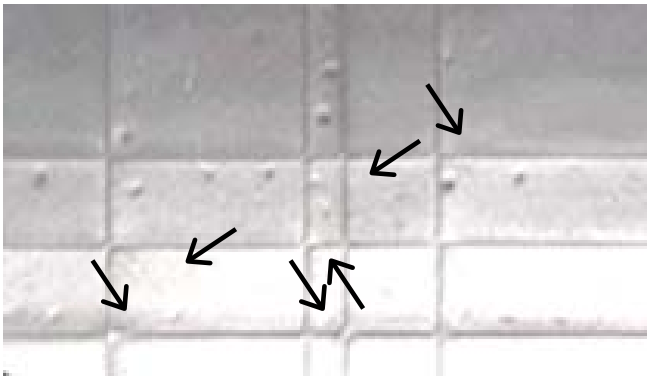

Fig. 3. A plan-view TEM micrograph of the sample with Ge SAQDs grown on the relaxed $Si_{0.85}Ge_{0.15}$ buffer layer is shown.

2). **Ge SAQDs on partially relaxed SiGe buffer layers:** Based on a modified partially relaxed SiGe buffer layer, instead of trying to achieve rectangular arrays of SAQDs without any random nucleation, we intentionally control the spacing between misfit dislocations to be much larger (on the order of 10 μm) than the diffusion length of Ge adatoms for the duration of the experiment. Such a buffer layer is an excellent vehicle for observing the detailed process of nucleation and growth of Ge SAQDs on Si (001). There are three types of sites on the surface of the relaxed buffer layer, over the intersection of two perpendicular dislocations (A), over a single dislocation line (B), and regions far away from any dislocation (C). The difference between the three types of sites is the misfit strain in the dots. The misfit strain is the lowest at site A and highest at site C. The difference in misfit strain translates into gradients in the chemical potential for Ge adatoms. The same difference also lead to altered free energy balance for SAQDs in terms of their shape.

The observation of three-stage nucleation:

AFM topography of samples with Ge coverage of 4.0, 4.5, 5.0 and 6.0 Å are shown in Fig. 4 (a)-(d). The first three images clearly illustrate the existence of three types of surface sites and the resulting three-stage nucleation at dislocation intersections [type A, (a)], single dislocation lines [type B, (b)], and in regions far away from dislocations [type C, (c)], respectively. Three-stage nucleation is clearly shown as the Ge coverage increases. At 4.0 Å, Ge SAQDs of pyramidal shape nucleate exclusively at A sites. These pyramids form a rectangular array with perfect registry to the network of buried dislocations. The pyramids show an aspect ratio of around 1:15 (±1) representing slightly lower angled facet than the well-known {105}. Additional 0.5 Å of Ge growth causes complete transition of the Ge islands from pyramids to domes (aspect ratio of ~1:10) at site A and the preferential nucleation of Ge SAQDs over dislocation lines (site B). Fig. 1 (b) shows a large rectangle bordered by dislocations consisting of SAQDs formed at A and B sites. Although the Ge coverage at this point is approximately the wetting-layer thickness (established in the literature to be ~3ML ≈ 4.2 Å in the case of Ge grown on bulk Si (001) substrate [[1]]), it is important to notice that there is no SAQD in the region between dislocations. The dislocation spacing of ~15μm is much larger than surface diffusion length of Ge adatom reported in

[1] Y.-W. Mo, D.E. Savage, B.S. Swartzentruber, and M.G. Lagally, Phys. Rev. Lett., 65, 1020 (1990)

literature [2,3] under similar conditions. The appearance of SAQDs at sites A and B indicates that either the Ge adatom density is higher or the nucleation barrier is lower at these sites.

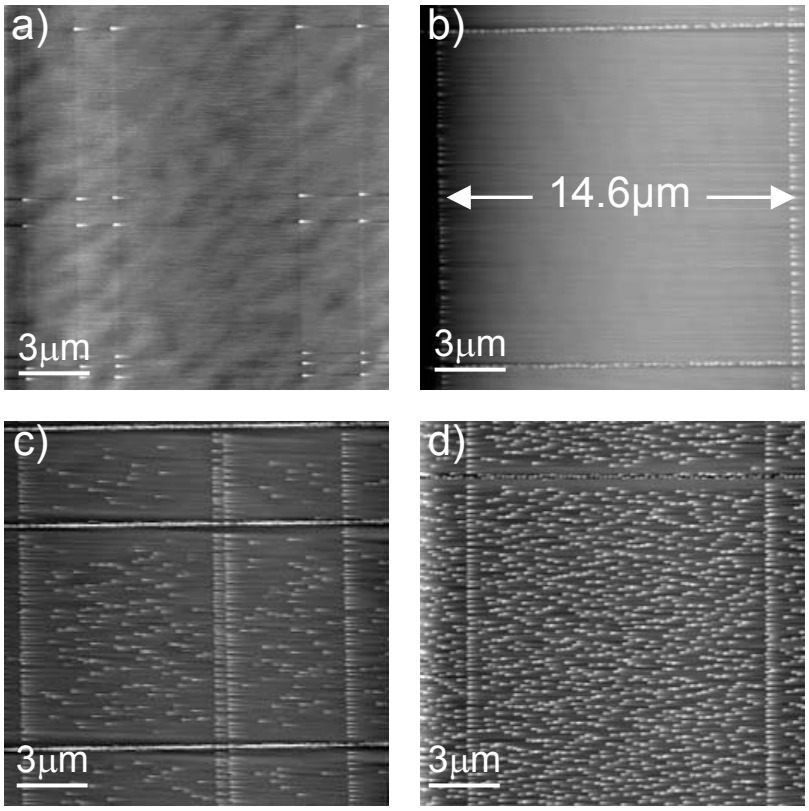

Fig. 4. Two-dimensional AFM topographic images of Ge SAQDs with 4-6 Å coverage on a partially relaxed $Si_{0.9}Ge_{0.1}$ buffer layer.
(a) 4.0 Å Ge coverage with Ge SAQDs only at site A
(b) 4.5 Å Ge coverage with Ge SAQDs at site A and site B
(c) 5.0 Å Ge coverage with Ge SAQDs at site A, site B, and site C
(d) 6.0 Å Ge coverage with Ge SAQDs at site A, site B, and site C

The pre-nucleation stage:

In an effort to differentiate between the two possibilities, surface topography immediately prior to the nucleation of any islands was examined in detail. Evidence of a higher density of Ge adatoms is observed at site B in the form of a ridge (not islands) of very low aspect ratio as shown in Fig. 5. The ridge height in samples with 3.0 Å Ge coverage was determined to be 9.0 ± 2.0 Å, a significant increase from the 3.5 ± 1.0 Å value in the sample with no Ge coverage. The original ridge height from samples with no Ge coverage agrees well with the observation by Lutz et al [4] who claimed a ridge height of 2.5 ± 0.3 Å for individual buried

[2] X. Deng, J. D. Weil, and M. Krishnamurthy, Phys. Rev. Lett., 80, 4721 (1998)
[3] T. Schwarz-Selinger, Y. L. Foo, David G. Cahill, and J. E. Greene, Phys.Rev. B 65, 125317 (2002)
[4] M.A. Lutz, R.M. Feenstra, F.K. LeGoues, P.M. Mooney, and J.O. Chu, Appl. Phys. Lett., **66**, 724 (1995)

dislocations. Although there are definite non-planarity at these sites, (001) remains to be the prevailing facets. The average terrace width of ~240 Å calculated from the aspect ratio of the ridges is comparable to that on

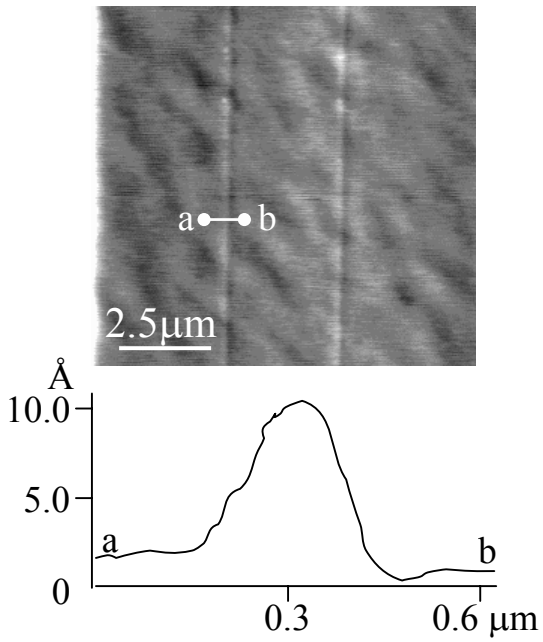

Fig. 5. Two-dimensional AFM topographic image of the sample with 3.0 Å Ge. Line scan of a-b illustrates that ridge height across buried single dislocation is 9.0 ± 2.0 Å.

typical Si (001) surfaces. The only difference is the polarity of the "force dipole" at these steps [5] are more aligned. We call these ridges "pile-ups" of Ge in order to differentiate them from SAQDs. The lack of 3-D Ge islands at this Ge coverage indicates that the wetting-layer thickness (> ~6 Å) at these sites is much thicker than at site C, presumably due to much reduced misfit strain at these sites. The above observation favors the higher Ge adatom density possibility over that of a lower nucleation barrier at B sites.

Similar "pile-up" of Ge is also observed at site A. There, due to the four-fold symmetry, the "pile-ups" are in pyramidal shape with extremely low (~1:200) aspect ratio. Furthermore, the aspect ratio seems to vary continuously with time, instead of staying at a constant value such as in the case of typical Ge pyramids on Si. The fact that no single facet is preferred indicates that such "pile-ups" of Ge are not SAQDs. In other words, they do not represent energetically stable islands. Instead, they could be explained by the existence of a chemical potential gradient for Ge adatoms toward A and B sites caused by the undulating strain field. Supporting this believe is the fact that such pile-ups are never observed at site C, where there is no directional diffusion of Ge adatoms.

The observation of simultaneous SAQDs growth and nucleation:

Ge coverage beyond 4.5 Å causes the adatom density at site C to reach the super-saturation level for 3-D island nucleation. At 5.0 Å Ge, randomly distributed SAQDs with rather low

[5] O. L. Alerhand and E. J. Mele, Phys. Rev. B **35**, 5533 (1987)

density (~2.3×10^8 cm^{-2}) appear at site C [Fig. 4 (c)]. Subsequent Ge growth causes the line density at site B to increase to a maximum value of ~5.5×10^4 cm^{-1}. There is a corresponding areal density increase at site C to ~6.0×10^8 cm^{-2}. Interestingly, the maximum SAQD density at site B and C are both reached at the Ge coverage of 6.0 Å. The dot density remains constant upon continued deposition of Ge from 6.0 to 8.0Å. In other words, there exists a period during the growth (that corresponds to Ge coverage between 6.0 to 8.0 Å under the current experimental condition) when the Ge adatom super-saturation falls below the value for nucleation of Ge islands. This happens when the incident Ge flux can no longer replenish the loss of Ge adatoms due to surface diffusion in regions between dots. Beyond 8.0 Å Ge coverage, coarsening sets in that will be discussed in the following part.

Different determining factors for the inter-dot spacing at different sites:

It is worth noting that the spacing between Ge SAQDs at site B is significantly smaller than that at site C. For example, in the sample with 6.0 Å Ge [Fig. 4 (d)], the spacing between dots at site B of ~0.03 μm is about an order of magnitude smaller than the value of ~0.4 μm at site C. One possible reason contributing to this difference is the anisotropic nature of strain in the dots at site B. The misfit strain between the dots and the substrate is less in the direction perpendicular to the underlying dislocation lines. It is not clear as to why the dots are so closely spaced. However, the close spacing indicates that there is strong elastic interaction between dots via the substrate. In other words, the dot spacing is likely to be determined by the interaction via the elastic strain field in the near surface region of the substrate. This is in clear contrast with the much larger spacing between dots at site C. At site C, the spacing between dots is determined by the surface diffusion length of Ge adatoms. The spacing varies with the substrate temperature in an Arrahnius fashion as shown in Fig 4. The activation energy extracted from such Arrahnius behavior is approximately 0.68 ± 0.04 eV, in close agreement with the well established value for surface diffusion of Ge on Si [6,7]. This observation provides strong evidence that the spacing between dots at site C is determined by surface diffusion of Ge adatoms.

The evidence for difference in misfit strain among SAQDs at different sites:

Finally, the critical size of pyramid-to-dome transition is used for qualitative comparison of misfit strain in SAQDs at sites A, B, and C. The critical size is characterized by the base diameter of the smallest domes and the largest pyramids. Ross et al [8] proposed that the transition represents the cross over of the free energy island shape from that of low angle facets to that consists of a multitude of larger angle facets. As a result, the critical size should be dependent on, and can be used as an indicator of, the misfit strain in SAQDs. The critical sizes at the three different sites can be measured experimentally at Ge coverage of slightly below 6.0 Å for which both pyramids and domes coexist. The critical sizes of SAQDs at sites A, B, and C are determined to be 2080 ± 10 Å, 1750 ± 10 Å, and 1490 ± 10 Å, respectively. This observation provides indirect evidence that the misfit strain is the lowest at site A and the highest at site C.

The observation of a rare event of SAQDs form after a single propagating dislocation:

---

[6] D. Srivastava and B. J. Garrison, Phys. Rev. B 46, 1472 (1992)
[7] C. Roland and G. H. Gilmer, Phys. Rev. B 47, 16286 (1993)

[8] F.M. Ross, J. Tersoff, and R.M. Tromp, Phys. Rev. Lett., **80**, 984 (1998)

During our study, we came across a rare event that is we believe the result of dot formation along a buried dislocation half loop that is expanding. In Fig. 6 the nucleation of Ge SAQDs proceeds from point A to B along buried single dislocation. Dot size becomes smaller while their spacing becomes larger as we move from the center towards the end of the dislocation half loop. This trend is symmetric towards the other end. Three line scans reveal that ridge heights of a-b, c-d, and e-f are 12 Å, 8 Å, and 3.5 Å, respectively. This trend indicates that the accumulation of Ge by surface diffusion happens at a finite rate. The time it takes is comparable to the time it takes for the dislocation to expand by several μm. As a result, the time period during which directional surface diffusion happens is noticeably shorter near the end of the buried dislocation half loop comparing to that near the center. The ridge height of e-f is comparable to one in the sample without Ge growth, whereas that of a-b is practically the value measured across any buried dislocation line in Fig. 4 (a) or (b). The ridge height rapidly decreases beyond e-f and becomes not measurable at the point ~5.5 μm past the last island. Total length of this propagating buried dislocation is found to be ~40 μm by the measurement of ridge height. Apparently, the dislocation half loop was introduced near the beginning of the Ge growth that took place at 700 ºC. Such a substrate temperature is sufficient to allow a dislocation half loop to grow at a rate that is on the order of a few μm per minute [[9]]. The formation of the dots along the line is practically trailing the expanding dislocation, allowing us to observe such a dynamic process unfold.

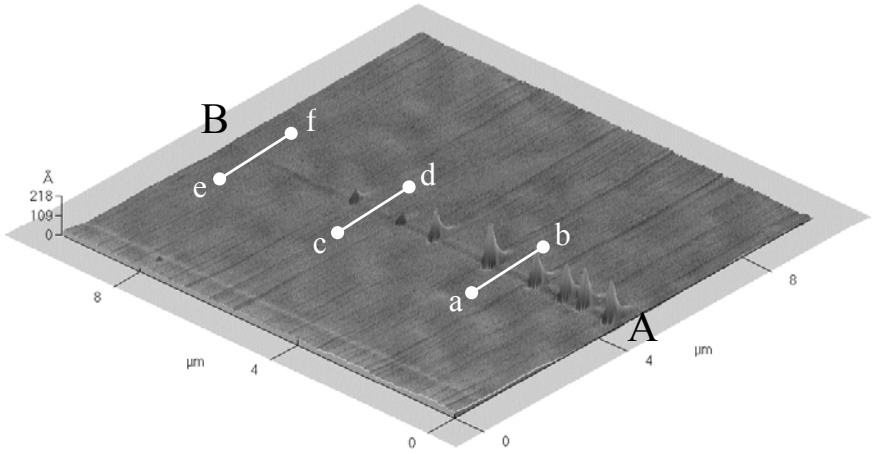

Fig. 6. Three-dimensional AFM topographic images of the sample in which the nucleation of Ge SAQDs proceeds along an underlying dislocation. Ridge heights across single dislocation of a-b, c-d, and e-f are ~12 Å, ~8 Å, and ~3.5 Å, rspectively.

The observation of the variation of denuded zone width with the temperature

Two-dimensional AFM topographic images of 6.0Å Ge coverage grown at five different temperatures on partially relaxed $Si_{0.9}Ge_{0.1}$ buffer layers are shown in Fig. 7. Dot-free denuded zone exists on both sides of buried dislocations along the two <110> directions. Furthermore, the denuded zone is wider as the growth temperature of Ge SAQDs increases, indicating the increase of surface diffusion coefficient. It is important to note the necessity of using properly designed relaxed SiGe buffer layers with dislocation spacing larger than the surface diffusion length of Ge adatoms. Failure to do so will lead to the absence of random dots,[[10]] and with that, plenty of useful information. Fig. 7 (f) shows no preferential

[9] R. Hull, J.C. Bean, D.J. Werder, and R.E. Leibenguth, Appl. Phys. Lett., **52**, 1605 (1988)
[10] Y.H Xie, S.B. Samavedam, M. Bulsara, T.A. Langdo, and E.A.Fitzgerald, Appl. Phys. Lett., **71**, 3567 (1997)

nucleation of Ge SAQDs over dislocations presumably due to the fact that the surface diffusion length of Ge adatoms is too short to be influenced by the chemical potential gradient over buried dislocations.[[11]] Particularly, incident Ge flux is expected to be drastically higher than the flux of diffusing Ge adatoms on the surface before the formation of SAQDs. Super-saturation abruptly decreases with the nucleation of large number of SAQDs. The average surface diffusion length is the longest for the sample in Fig. 7 (e) that is grown at the highest growth temperature (750 °C) with the slowest growth rate (0.05 Å/sec). Therefore, more Ge adatoms incorporate into the region over buried dislocations and the probability of the nucleation of random SAQDs decreases due to the lack of Ge adatoms. Eventually larger denuded zone forms compared to the other samples grown at lower growth temperature or higher growth rate. The AFM images of Fig. 7 (e) and (j) show the relatively non-uniform size distribution of SAQDs located over buried dislocations. Coarsening (Ostwald ripening) is believed to cause the broader size distribution as well as the larger average size of SAQDs at the expense of the decrease of dot density.

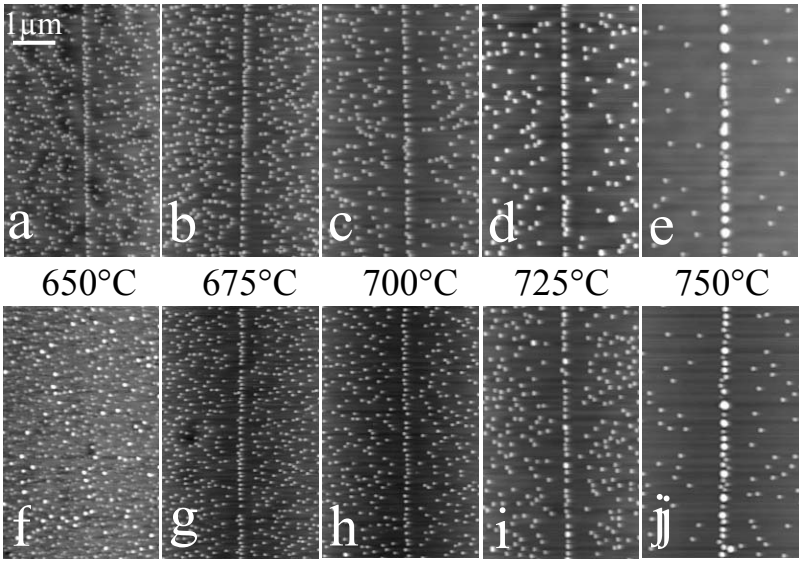

Fig.7 Two-dimensional AFM topographic images of 6.0Å Ge coverage grown at five different growth temperatures on partially relaxed $Si_{0.9}Ge_{0.1}$ buffer layers in which buried dislocations provide the preferential nucleation sites. The growth rate of low-temperature Ge wetting-layer (3.4 Å) is 0.05 Å/sec. Subsequent 2.6 Å Ge are grown at 0.05 Å/sec for (a)-(e) and at 0.1 Å/sec for (f)-(j). Particularly, (e) and (f) show two extremes caused by high and low surface diffusion coefficients, respectively.

Calculation of the activation energy and surface diffusion coefficient

A separate study reveals that for a given temperature the density of random SAQDs increases with dislocation spacing, starting from an absence of random SAQDs at small separations (that is, completely preferential nucleation over dislocations) to a saturation value for widely spaced dislocations. This behavior at four different growth temperatures is clearly shown in Fig. 8. The dot densities at the saturated stage are not dependent upon the chemical potential gradient over buried dislocations. Therefore the surface diffusion of adatoms is dominant factor determining the dot densities. Fig. 9 shows Arrhenius plot of the areal

[11] H.J Kim, Z.M. Zhao, and Y.H. Xie, Phys. Rev. B **68**, 205312 (2003).

density of random SAQDs in the region away from dislocations as a function of the growth temperature between 650 ºC and 750 ºC. The areal dot densities are obtained from the saturated stage. The figure shows near perfect Arrhenius behavior from all samples grown at 650 ºC as well as 750 ºC with one exception. The only data point that deviates significantly is grown at 750 ºC with the low growth rate of 0.05 Å/s. We believe that the deviation is a result of the extremely long surface diffusion length of Ge adatoms on the surface leading to non-negligible coarsening. The apparent spacing between dots increases when smaller dots disappear as a direct consequence

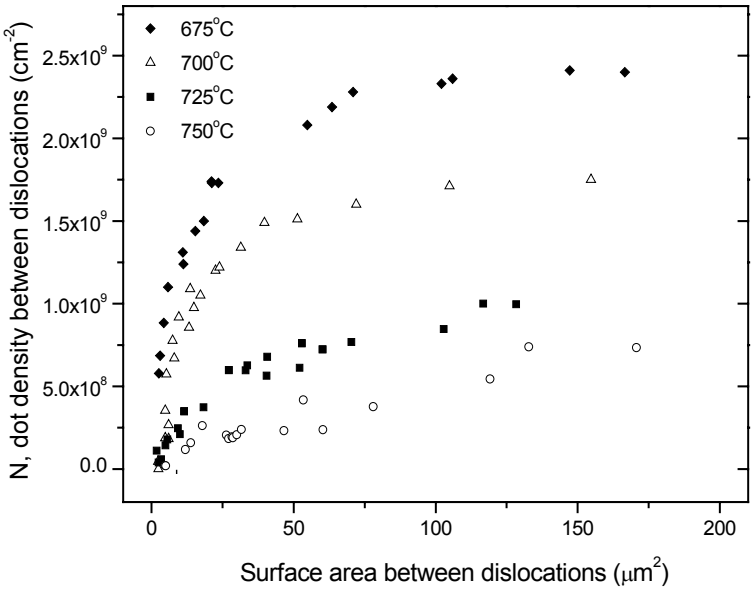

Fig. 8. The evolution of dot areal density as a function of the surface area between dislocations.

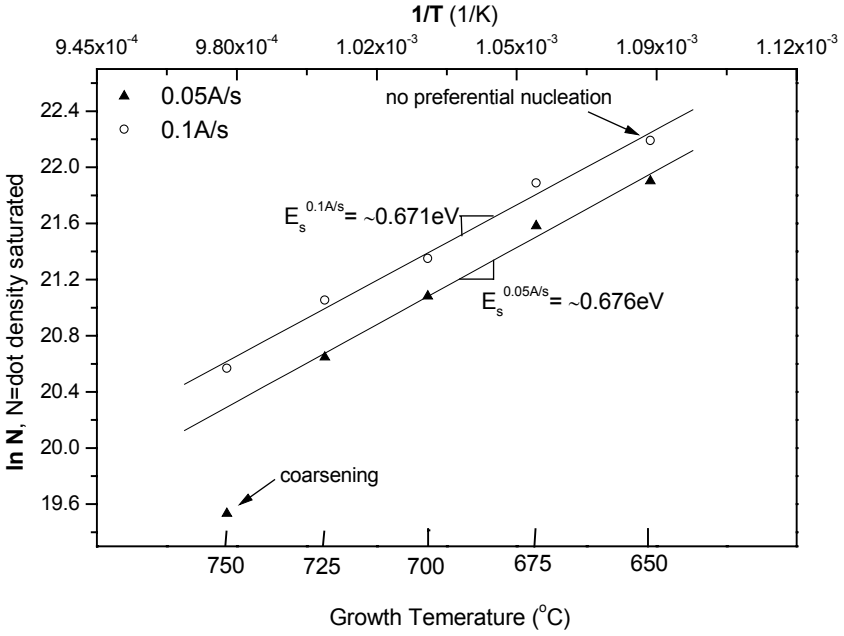

Fig. 9. Arrehenius plots of the areal density of randomly nucleated dots in the region between dislocations versus the growth temperature.

of coarsening. Based on the equation of $N \propto \exp(2E_s / k_B T)$, the activation energies obtained from two different growth rates of 0.05 Å/sec and 0.1 Å/sec are 0.676 ± 0.03 eV and 0.671 ± 0.03 eV, respectively. The two values agree very well with one another. The experimental activation energies are comparable to the ones calculated in the literature[12,13]. We take this as an evidence that it is indeed directional diffusion that leads to the observed denuded zone.

Now we obtain the pre-exponential factor from the volume increase of SAQDs over dislocations. Additional two samples with 5.0 Å Ge coverage (3.4 Å wetting-layer plus 1.6 Å Ge SAQDs in a two-step growth) were grown at 700 ºC with growth rates of 0.05 Å/s and 0.1 Å/s, respectively. The average volumes of SAQDs were carefully measured to compare with two other samples with 6.0 Å Ge coverage. At this growth temperature the dot size distributions are found to be relatively uniform at positions over buried dislocations and in the region away from dislocations. Moreover, no coarsening effect is observed at two different Ge coverages. The average volume of SAQDs over buried dislocations is apparently larger than that in the region away from dislocations. It has been known that much more Ge adatoms are incorporated into the region over buried dislocations due to the chemical potential gradient. The volume increase of SAQDs over dislocation is approximately proportional to the denuded zone width and larger than that of those in the region away from dislocations. We found that the total number of Ge atoms impinging onto the denuded zones is slightly larger than that for the average volume increase of SAQDs over dislocations at both growth rates. This is an evidence that the majority of Ge adatoms incident within the denuded zone incorporates into the existing SAQDs over dislocations between 5.0 Å and 6.0 Å Ge coverage. Furthermore, the line density of SAQDs over dislocations is identical at two Ge coverages with complete dome. This observation implies the absences of additional dot nucleation as well as pyramid-to-dome shape transition. Based on the simple assumption that there is a concentration gradient of Ge adatoms in the denuded zones caused by the chemical potential gradient, surface diffusion coefficient (D_s) is calculated using Fick's first law.

$$J = -D_s \frac{\Delta n}{\Delta x} \qquad (1)$$

Flux J (atoms/sec) is given by the average volume increase of SAQDs over dislocation between two different Ge coverages of 5.0 Å and 6.0 Å. The number of Ge atoms impinging directly onto the existing SAQDs is negligible because the area of denuded zone on both sides is significantly larger than that occupied by SAQDs. $\Delta n / \Delta x$ (atoms/cm^2) is the number of Ge atoms landing onto the unit area of denuded zone. In the samples grown with a growth rate of 0.05 Å/s, the volume measurement reveals that ~7.1×10^5 atoms are used for the volume increase of an individual dot over buried dislocations for 20 seconds (2000 nm^3 ≈ 88400 Ge atoms). Based on the fact that 1.0 Å Ge coverage corresponds to ~4.48×10^{14} atoms/cm^2, it is found that ~8.0×10^5 atoms arrive onto the square region in the denuded

[12] D. Srivastava and B. Garrison, Phys. Rev. B **46**, 1472 (1992)
[13] C. Roland and G.H. Gilmer, Phys. Rev. B **47**, 16286 (1993)

zone. As a result, D_s = ~7.97 × 10^{-11} cm^2/sec. Using the well-known equation of $D_s = D_o \exp(-E_s/kT)$ and the activation energy (0.676 eV), a pre-exponential factor (D_o) is ~2.53 × 10^{-7} cm^2/sec. At the higher growth rate of 0.1 Å/s much smaller number of Ge atoms (~1.09 × 10^5 atoms) incorporate for the volume increase presumably due to the smaller denuded zones. Consequently, the volume increase of SAQDs over dislocations is considerably smaller compared to that of the sample with 0.05 Å/s. Using the activation energy (0.671 eV) obtained from the samples of 0.1 Å/s we obtain a slightly smaller pre-exponential factor (~1.0 × 10^{-7} cm^2/sec), implying a slower surface diffusion rate.

2. III-V quantum dots on Si (001):

1). Fabrication of InAs SAQDs on Si (001): Comparing to Ge SAQDs on Si, the considerations involved in the growth of InAs SAQD on Si is quite a bit more complex. Because there is only one group in the world headed by Prof. Bimberg and Prof. Gosele of Germany that is doing serious research in the fabrication of InAs SAQD on Si, there isn't much information available in the literature. For example, the most important question of whether the growth is in Stranski-Krastanov mode (a wetting layer followed by 3D growth) or Vomer-Weber mode (non-wetting 3D growth) is not known for sure. Furthermore, the effect of As over-pressure on the dot nucleation and shape is not established, although we have been growing in the As rich regime. Finally, the critical dot size for dislocation has not been determined.

For InAs coverage dependence study

Plan-view TEM images of InAs dots with different InAs nominal coverage are shown in Figure 1. The density and size dependence on InAs coverage are shown in Figure 2. TEM results indicate that dot formation begins at very early stage of the growth (< 0.3 ML). At 0.3 ML of InAs coverage, the dot density is approximately 1.7×10^{10} cm^{-2} indicating Volmer-Weber (VW) growth mode.

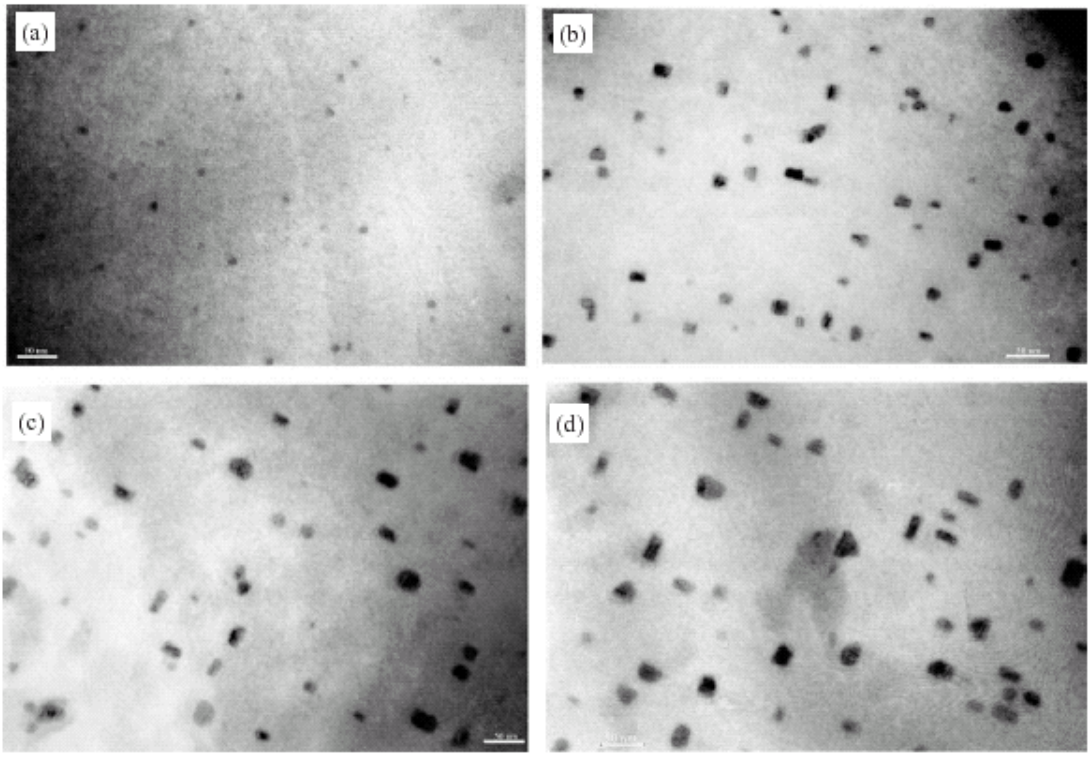

Figure 1. Bright-field plan-view TEM of InAs dots with various InAs nominal coverage (a) 0.3 ML, (b) 0.7 ML, (c) 1.0 ML, (d) 1.4

ML.

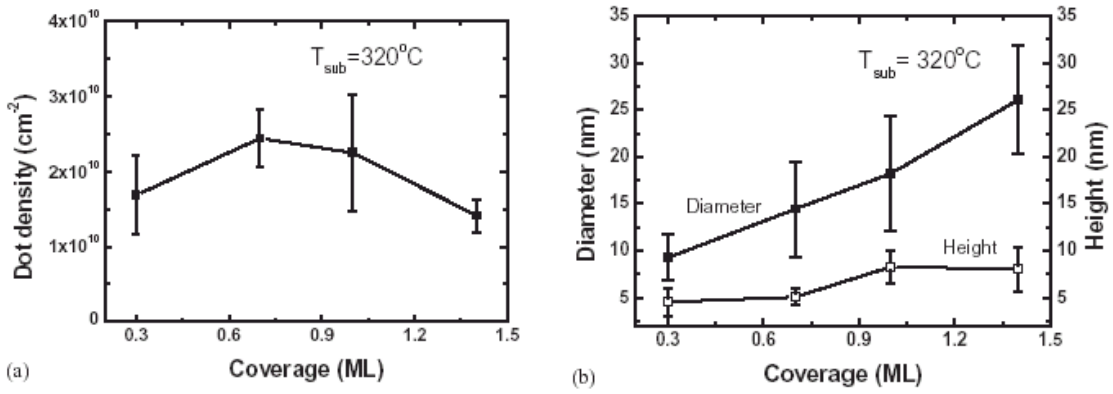

Figure 2. (a) Plot of InAs dot density dependence on the nominal coverage and (b) Plot of InAs dot size dependence on the nominal coverage.

Figure 3 shows the cross-section TEM of typical InAs dots with the different coverage. With increasing InAs coverage, not only dot size but also shape of the dots change. Most dots have an irregular shape at 0.3 ML coverage that changes to highly regular huts with (111) facets at 0.7 ML. At 1.0 ML, portion of dots evolves into dome shape with no clear facets. At 1.4 ML, nearly 100% of the dots are dome shape.

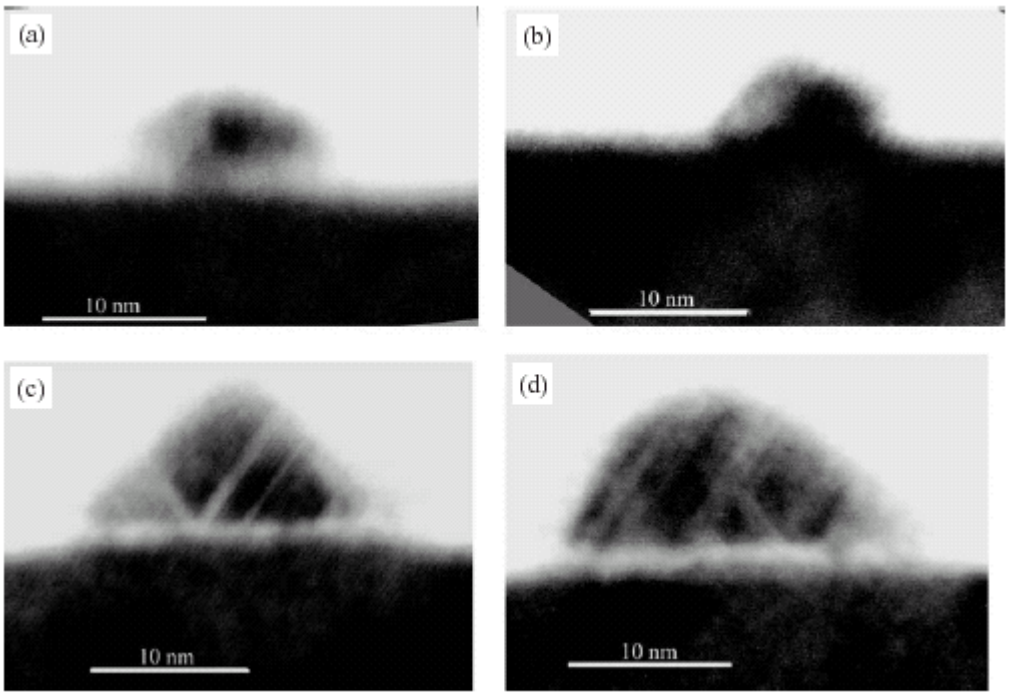

Figure 3. Bright-field cross-section TEM of typical InAs dots with different InAs nominal coverage: (a) 0.3 ML, (b) 0.7 ML, (c) 1.0 ML, (d) 1.4 ML.

For arsenic pressure dependence study

The strong dependence of dot density on As BEP is in clear contrast to its weak dependence on InAs coverage, as shown in Figure 4(a). InAs dot density increases in a near exponential fashion from 4.3×10^{9} to 1.8×10^{11} cm^{-2} as As BEP is decreased from 9.2×10^{-6} to 1.2×10^{-7} torr.

InAs dot size and volume change with decreasing As BEP, as shown in Fig. 4(b). The total dot volume decreases at the low As BEP. This indicates that there are 2-dimensional InAs structures formed between dots at low As BEP.

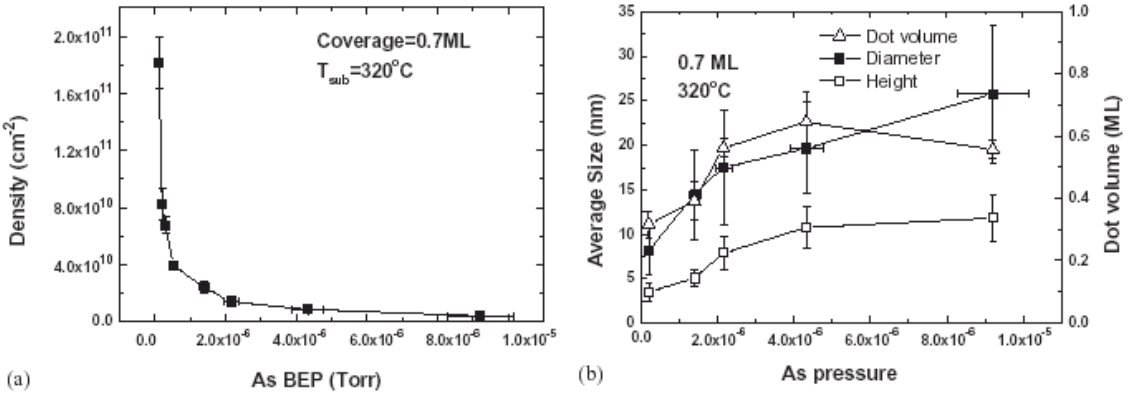

Figure 4. (a) Plot of InAs dot density dependence on arsenic BEP, (b) Plot of InAs dot size and volume dependence on arsenic BEP.

The well-reconstructed 2x1 surface completely disappears after InAs growth at low As BEP, indicating a highly "defective" As monolayer, i.e. with high density of As vacancies, as shown in Figure 5. The fact that high InAs dot density is obtained only at low As BEP supports the proposed mechanism.

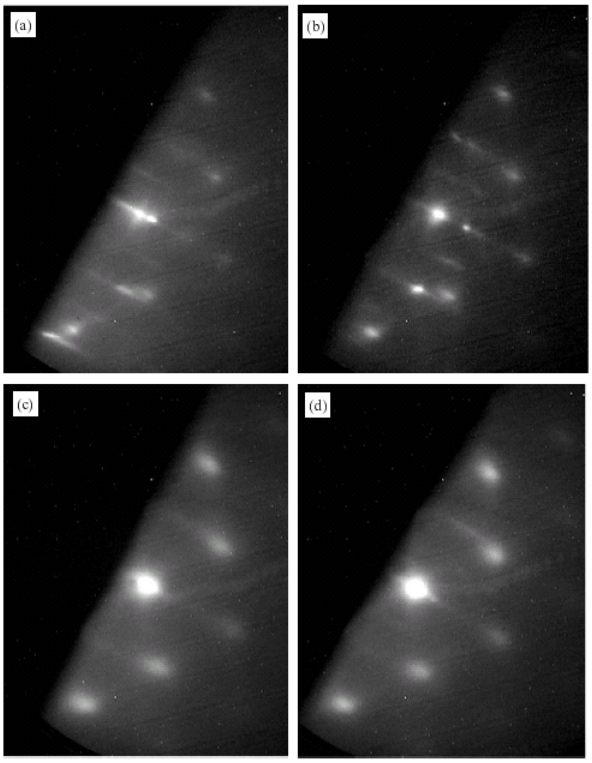

Figure 5. RHEED pattern of InAs growth with different arsenic BEP: a) 9.2×10^{-6} torr, b)1.4×10^{-6} Torr, c) 3.0×10^{-7} Torr, d) 1.2×10^{-7} Torr.

For temperature dependence study of dot formation,

The left side of figure 6 shows bright-field plan-view [001] TEM micrographs of samples grown at different substrate temperatures increased from 295 ^{o}C for a) to 410 ^{o}C for e). The

right side of figure 6 is the histogram of size distribution based on the plan-view TEM. Gaussian curves were fitted on the size distribution histogram of figure 6. It is clear that increasing substrate temperature results in broadening of dot size distribution. Gaussian peak width, referd to as 0.849 full-width at half maximum (FWHM), increases from 8 nm to 14 nm when substrate temperature increases from 295 ^{o}C to 410 ^{o}C. Coarsening is likely to be responsible for the broadening of dot size distribution.

Figure 7 shows the dependence of dot density on substrate temperature. Dot density is nearly independent of substrate temperatures. The dot density at the onset of nucleation can be written for the well-studied quantum dot systems such as Ge/Si and InAs/GaAs [14,15] as follows[16]:

$$n \propto \left(\frac{F}{D_s}\right)^{\alpha} \qquad (1)$$

where F is the growth flux coming from source, D_s is the surface diffusion coefficient which increases exponentially ($D_s=D_0 exp(-E_a/k_BT)$) with increasing temperature. α is a constant associated mainly to the critical cluster size. α increases with increasing cluster size and saturates at unity for critical cluster size larger than 10 atoms. [17] For epitaxial growth, α can be treated as a constant.[14,15] n in equation (1) is the initial dot density. This simple model cannot explain the experimental observation that the dot density is nearly independent of temperature within the range of 295 ^{o}C to 410 ^{o}C under a constant arsenic BEP. This suggests that the nucleation model as in equation (1) that has been shown to be valid for Ge/Si and InAs/GaAs systems, does not apply to InAs growth on Si under our growth conditions.

[14] H. J. Kim, Z. M. Zhao, J. Liu, V. Ozolins, J. Y. Chang, Y. H. Xie, J. Appl. Phys. 95 (2004) 6065.
[15] K. Shiramine, T. Itoh, S. Muto, T. Kozaki, S. Sato, J. Cryst. Growth 242 (2002) 332.
[16] M. Schroeder, D. E. Wolf, Phys. Rev. Lett. 74 (1995) 2062.
[17] W. Theis, R. M. Tromp, Phys. Rev. Lett. 76 (1996) 2770.

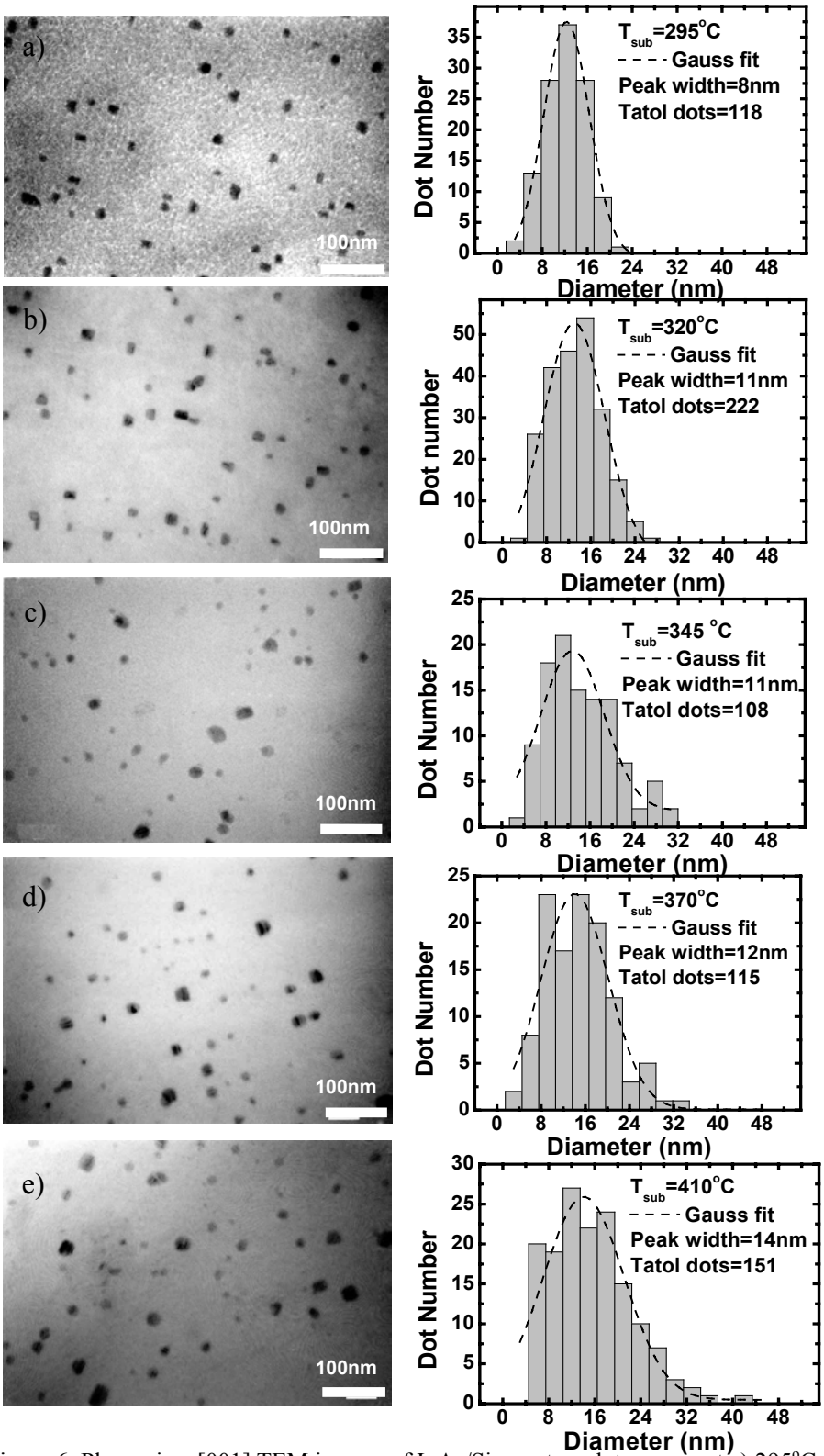

Figure 6. Plane-view [001] TEM images of InAs/Si quantum dots grown at a) 295°C, b) 320 °C, c) 345 °C, d)370 °C, e)410 °C.

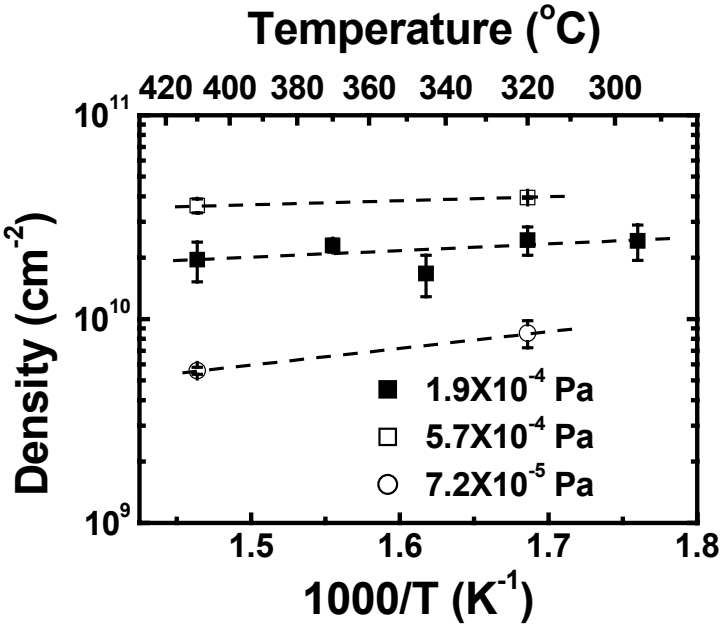

Figure 7. Arrhenius plot of InAs/Si dot density (y axis) dependence on substrate temperature (x axis).

Optimization of InAs quantum dots on Si.

High quality, narrow size distribution and high density dots can be achieved by InAs growth at lower temperature and lower arsenic BEP. In order to improve crystal quality and avoid the indium segregation under high temperature treatment, the dots growth is followed by annealing at higher temperature and higher arsenic BEP. The increase of RHEED intensity after growth and annealing, compared to samples grown at low temperature (below 250°C), confirmed the improvement of crystalline quality. Figure 8 (a) shows the plan-view TEM image of a sample that was grown at substrate temperature of 250°C with arsenic and indium BEP of 7.2×10^{-5} Pa and 7.6×10^{-6} Pa and annealed at substrate temperature of 410 °C with arsenic BEP of 1.9×10^{-4} Pa. The ramping time from 250 °C to 410 °C was set to 5 minutes. After the 120 second annealing at 410°C, the sample was cooled down to room temperature in approximately 10 minutes. This growth procedure resulted in QD density of 5.7×10^{10} cm^{-2}. The size distribution is shown in figure 8 (b). The Gaussian curve fitting of size distribution gives a narrow peak at around 11 nm with Gaussian peak width of 7 nm. The improvement in size distribution and the high density are attributed to low temperature growth and low arsenic BEP, respectively.

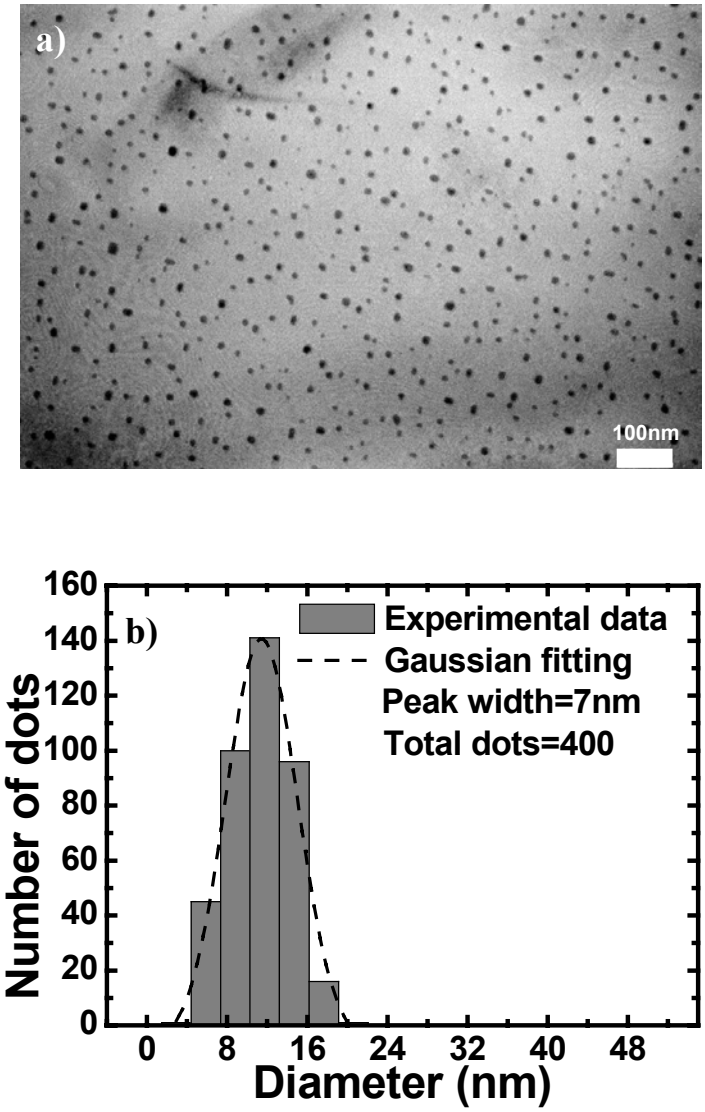

Figure 8. InAs dots grown on Si (100) at the substrate temperature of 250^{o}C and with arsenic BEP of 7.2×10^{-5} torr and post-annealed at 410^{o}C and 1.9×10^{-4} torr arsenic BEP: a) bright field plan-view [001] TEM micrograph and b) Histogram of size distribution of InAs dots.

InAs dot density dependence on III-V ratio:

InAs quantum dots were grown under different III/V ratio. The dot density change with III/V ratio is shown in the figure 9.

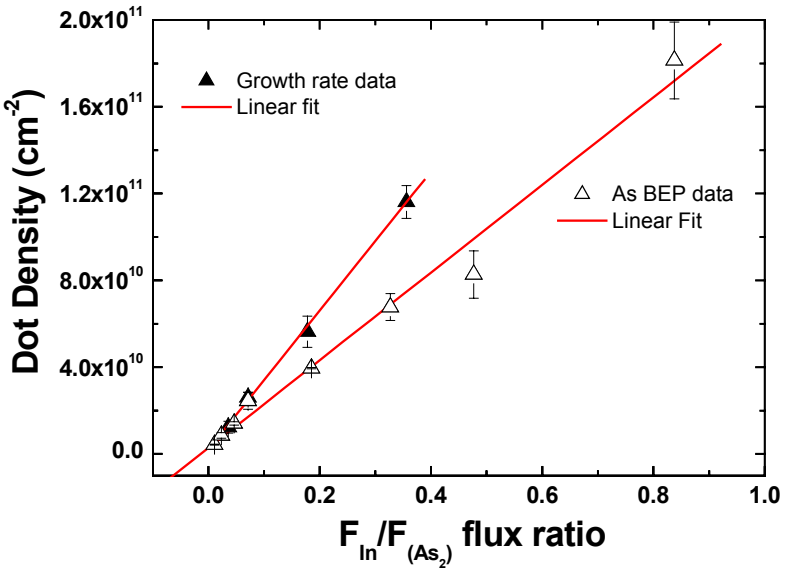

Figure 9. dot density dependence on III/V flux ratio. For the growth rate data the As BEP was kept at 1.4×10^{-6} Torr, for As BEP data growth rate was set at 0.02 ML/s. All growth was done at 320°C

The data from both constant As BEP and In BEP show the same trend that dot density is nearly linearly dependent on III/V flux ratio. This behavior provides a way to control the InAs dot density in a very large range from 10^9 cm^{-2} to 10^{11} cm^{-2}.

2). <u>Growth Mode of III-V on V substrate</u>

From the growth of GaAs, InAs on Si and GaAs on Ge, we conclude that they are all in Volmer-Weber growth mode. Fig. 10 showed the reflection high-energy electron diffraction (RHEED) for the early stages (below 1 ML) of GaAs on Si (a), InAs on Si (b), GaAs on Ge (c). Fig. 10 (d) and (e) showed the RHEED pattern of Si and Ge surface before growth. It is very clear that the 3-dimensional island growth at very early stage (below 1 ML). Therefore all of the growth are Volmer-Weber growth without 2-dimensional wetting layer growth. Fig. 11 showed the AFM pictures of GaAs 0.7ML on Si (a), InAs 0.7 ML on Si (b). AFM data confirmed 3-D Volmer-Weber growth.

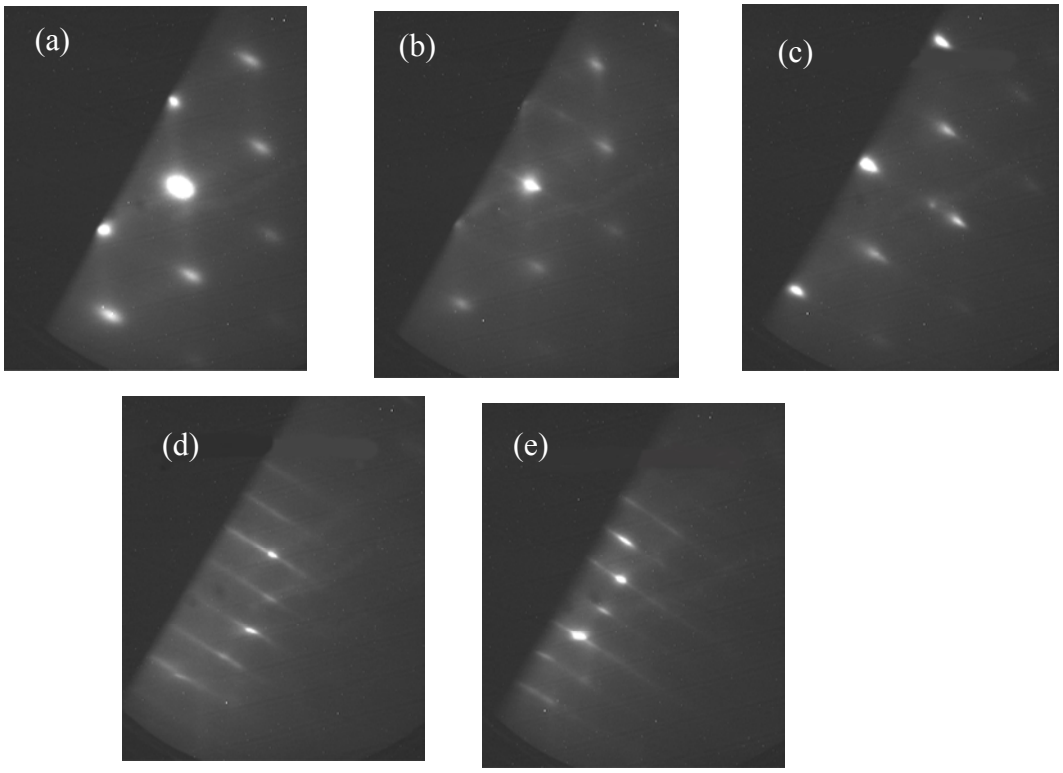

Fig. 10. RHEED images for different growth, (a)GaAs/Si at 320^{o}C, (b) InAs/Si at 320^{o}C, (c) InAs/Ge at 320^{o}C, (d) Si surface before growth, (e) Ge surface before growth.

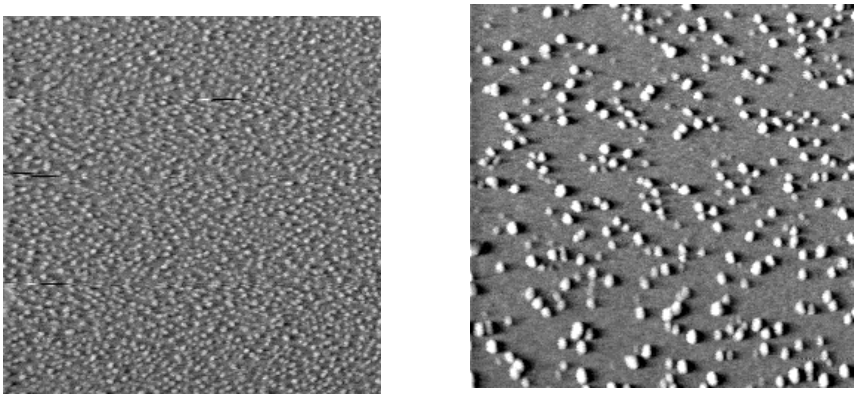

(a) (b)

Fig. 11. 1 ×1 μm^2 AFM of GaAs (a) and InAs (b) growth on Si at the initial stages at InAs/Si at 320^{o}C with arsenic BEP 1.4× 10^{-6} Torr.

3). First-principles calculations of different InAs overlayers on Si(001)

To understand the mechanism of initial stage of InAs grown on silicon (001) surface, first-principle total energy calculations were carried out with the plane-wave pseudopotential method within the generalized gradient approximation (GGA). A conjugate-gradient algorithm is used to minimizing the total energy therefore obtain the atom positions. Fig. 12 shows the positions of atoms in different systems with different InAs overlayers on silicon (001). We calculated the total energies of systems with different thickness of InAs on silicon substrate, which is shown in Table I. Comparing the total energy of two systems with the same number of atoms, while one system has half surface area covered with single As layer and half covered with As-In-As-In-As layer and another one with the whole surface covered with As-In-As layer, we can find the former one has a total energy of -(63.40+92.36)/2 eV = -77.88 eV, which is lower than the total energy (-77.82 eV) of system with a uniform As-In-As layer. For a system with 1/3 area covered with As-In-As-In-As-In-As and 2/3 with single As, the total energy is –(106.97/3+63.40×2/3) eV = -77.92 eV, which is even lower. So the system prefers to form InAs islands with As-finished silicon surface rather than uniform InAs layer on silicon surface, which causes a 3D growth mode of InAs on silicon even in the very initial stage. In the real case, since the island formation in 3D growth will partially release the strain energy that is comes from the lattice mismatch between InAs and Si, the 3D growth will be even more energy favorable.

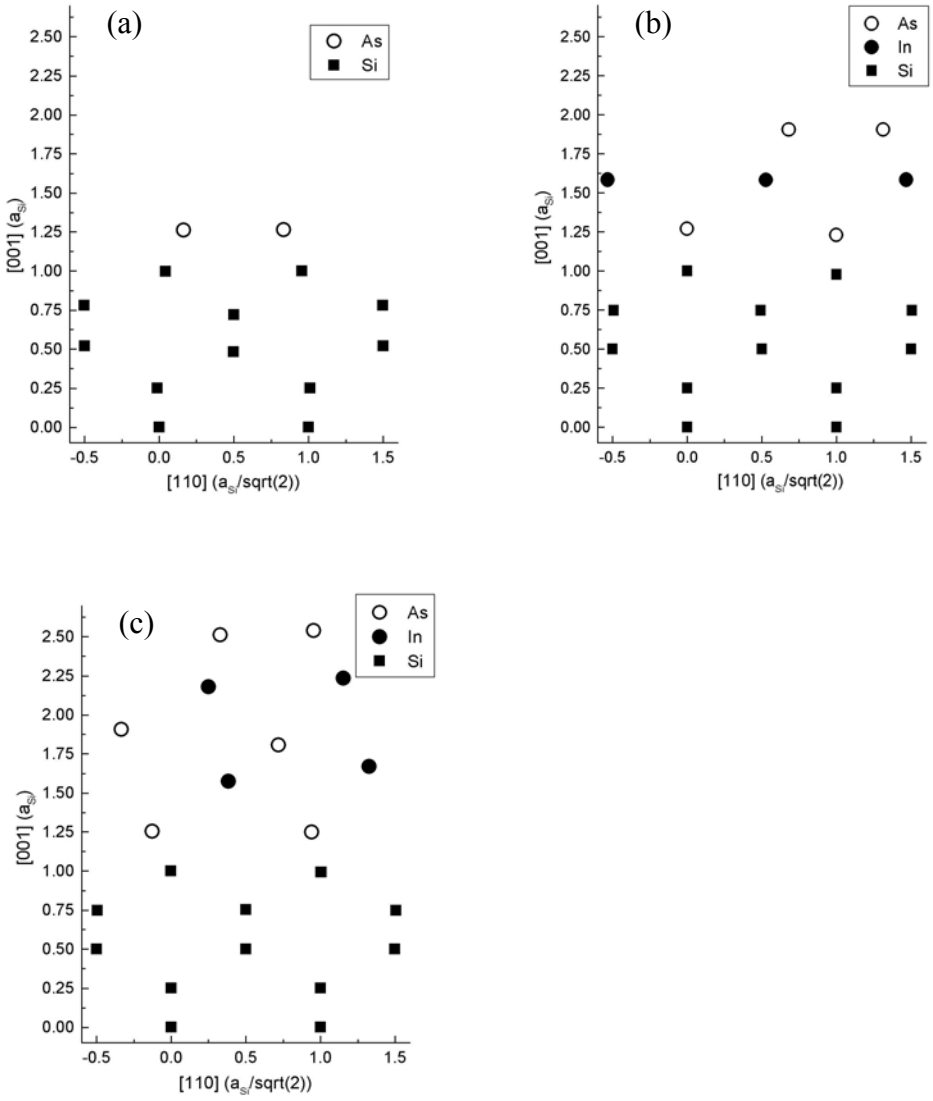

Fig. 12. Calculation positions of atoms in (a) Si(001)-As, (b) Si(001)-As-In-As and (c) Si(001)-As-In-As-In-As.

TABLE I. Total energies of systems with different InAs overlayers on silicon. The unit area used in the table is the area for one surface dimmer.

Structure	Total energy (eV/unit area)
Si(001)-As	-63.40
Si(001)-As-In-As	-77.82
Si(001)-As-In-As-In-As	-92.36
Si(001)-As-In-As-In-As-In-As	-106.97

4) Critical size of threading dislocation-free dots at different growth conditions:

1. Critical size dependence on arsenic BEP

Plastic relaxation in strained InAs islands grown on Si (001) by MBE as a function of arsenic beam equivalent pressure is investigated using transmission electron microscopy. Analyses of the spacing in Moiré fringes show a clear trend of larger InAs lattice parameters with increasing island size as a result of the elastic relaxation of three-dimensional structures. Our experimental findings show: (1) the existence of a critical lattice parameter (0.597 ±0.01nm) instead of a critical island size that determines the onset of dislocation, and (2) a clear dependence of the critical size of InAs clusters on arsenic BEP during MBE growths from 1.2×10^{-7} to 9.2×10^{-6} Torr. We postulate that these results are the consequences of the As BEP dependent surface energy of the various facets and the associated InAs island shape change.

Fig. 13 showed the dark-field plan-view TEM images of InAs dots grown under different arsenic BEP. The Moiré fringes of each dot can be accurately determined from images. The lattice parameters can be obtained from spacing of Moiré fringes.[18,19] The dislocation can be identified from the terminated Moiré fringe.[20]

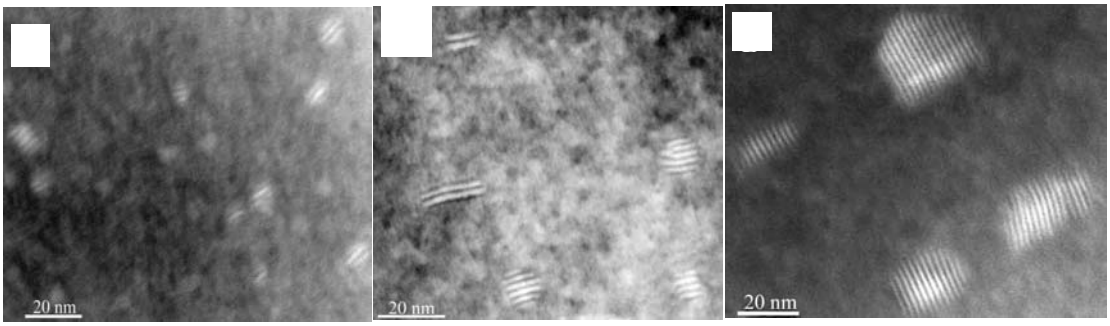

Fig. 13 Dark field (**g** = 220) plan-view TEM micrographs of InAs islands on Si (001) substrate with As pressure equal to 1.2×10^{-7} Torr (A), 1.4×10^{-6} Torr (B) and 9.2×10^{-6} Torr (C). Samples are grown at 320ºC with 0.7ML InAs coverage

The size distribution of both dislocation-free dots and dislocated dots was shown in Fig. 13. It is very clear that the relative percentage of relaxed versus strained islands increases monotonically with BEP_{As} (from 15% of dislocated InAs islands for the lowest As BEP to 70% for the highest As BEP)

---

[18] P.D. Miller, C.P. Liu, W.L. Henstrom, J.M. Gibson, D.G. Cahill, Y. Huang, P. Zhang, T.I. Kamins, D.P. Basile, R.S. Williams, Appl. Phys. Lett. 75 (1999) 46.

[19] P. Chen, Q. Xie, A. Madhukar, Li Chen, A. Konkar, J. Vac. Sci. Technol. B 12 (1994) 2568.

[20] "Electron Microscopy of Thin Crystals," P. Hirsch, A. Howie, R.B. Nicholson, D.W.Pashley, and M.J. Whelan, (Robert E. Krieger, New York, 1977), p.372.

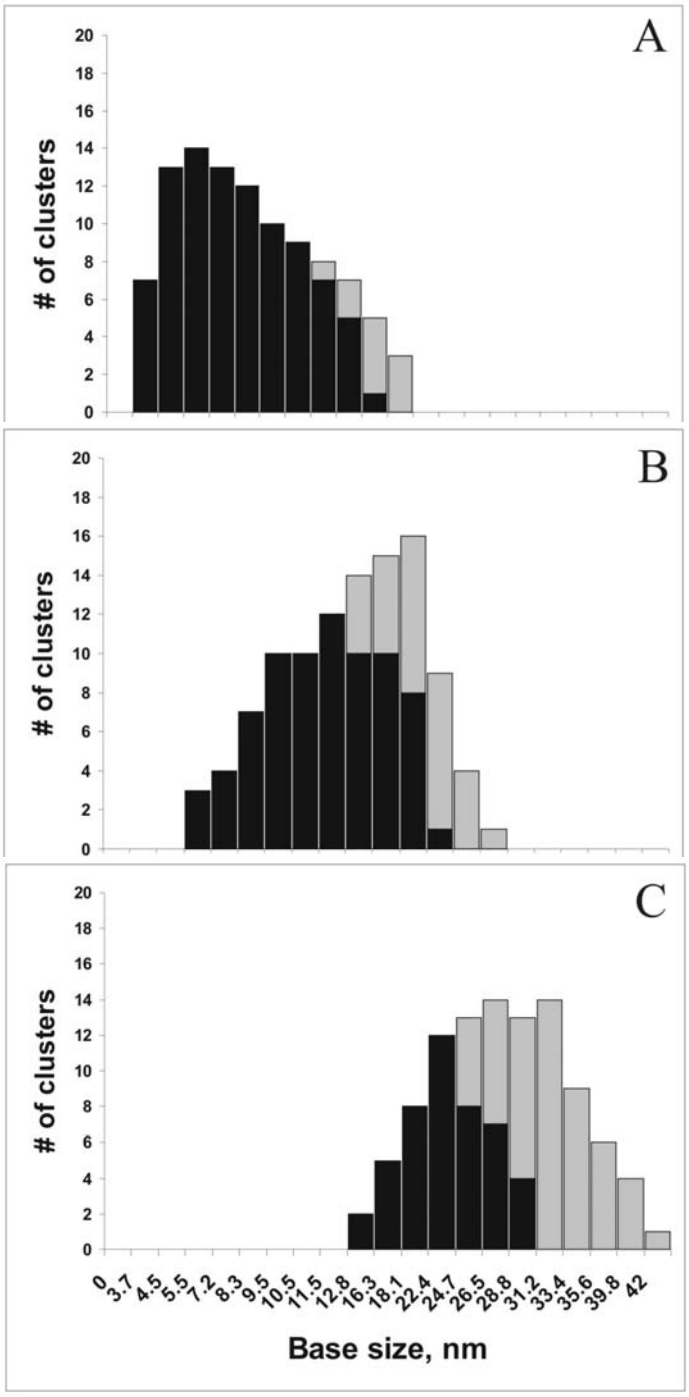

Fig 14. The histograms of dislocation-free (black) and dislocated (gray) islands as function of their base sizes corresponding to the same set of samples as in Fig.13.

The critical sizes of dislocation-free dots grown under different arsenic BEP are shown in Fig. 15. The critical base size dimensions of coherent islands increases significantly (from 13 to 28 nm) with increasing arsenic BEP from 1.2×10^{-7} Torr to 9.2×10^{-6} Torr.

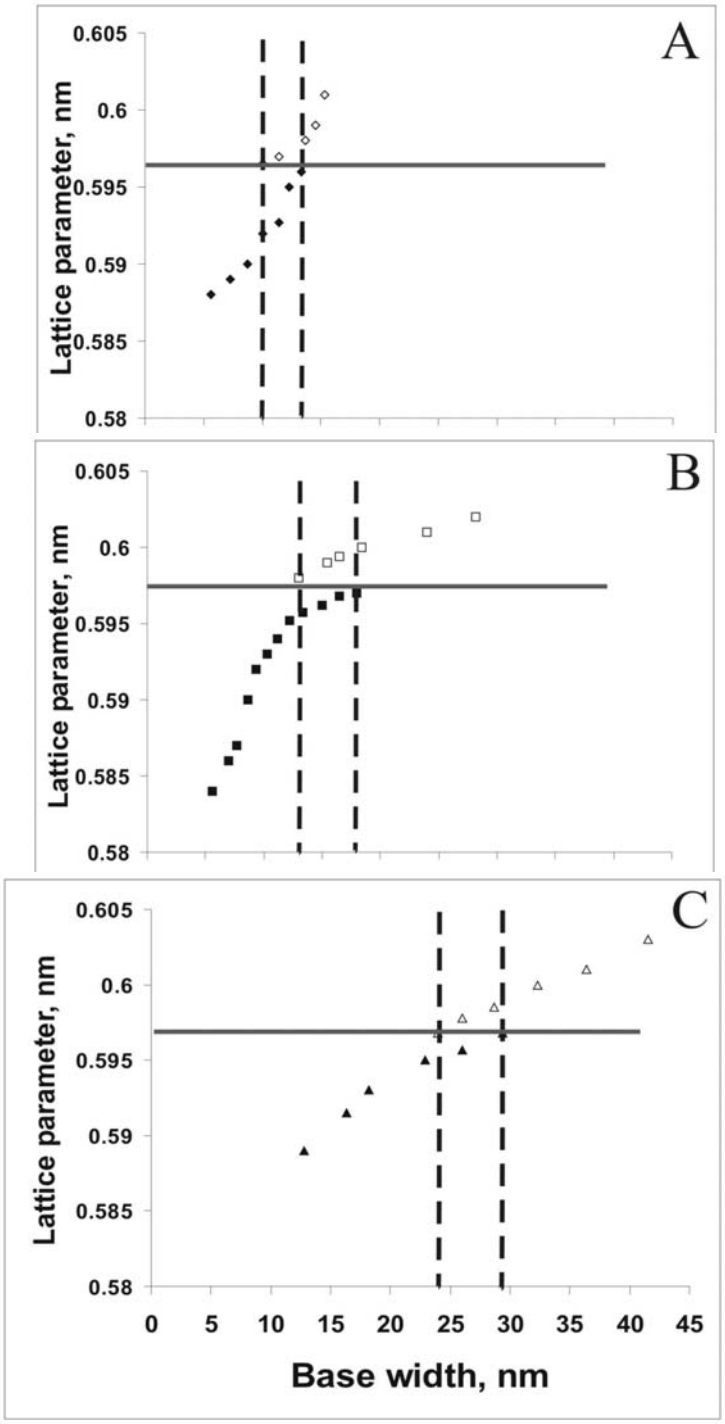

Fig. 15 The average in-plane lattice parameter of InAs islands as a function of their base sizes for the same set of samples as in Fig.13. Dislocation occurs at a well defined a = 0.597±0.01 nm (as indicated by horizontal lines) and is relatively independent of island sizes.

2. Critical size dependence on substrate temperature

Relaxation of InAs islands epitaxially grown by molecular beam epitaxy on Si (001) as a function of the substrate temperature is investigated using transmission electron microscopy. Analysis of the spacing in Moiré fringes shows that an increase in the average InAs lattice

parameters with increasing island sizes in both elastically as well as plastically relaxed islands. Using this method, a critical InAs islands size for dislocation is determined to be 13.5±0.1 nm, with a corresponding critical InAs lattice spacing of 0.579±0.01nm along ⟨011⟩ crystallographic directions. The critical dimensions are independent of the substrate temperature. Although no dislocations can be observed in islands smaller than the critical size, the size of the largest dislocation-free islands does increase significantly (from ~17 nm to ~24 nm) with increasing substrate temperature (from 295ºC to 410ºC).

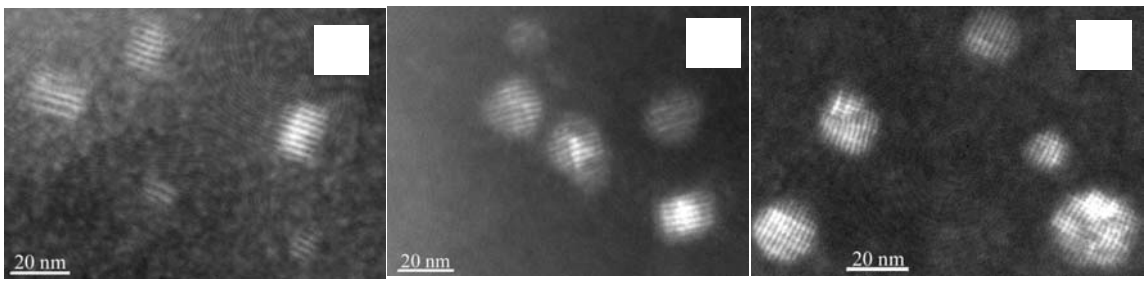

Fig.16 Dark field (**g** = 220) plan-view TEM micrographs of InAs islands on Si (001) substrate for samples grown with As pressure equal to 1.4×10^{-6} Torr with total coverage 0.7ML at substrate temperatures 295ºC (A), 345ºC (B) and 410ºC (C), respectively.

Fig.16 shows typical plan-view TEM micrographs of samples grown at three different temperatures: 295ºC, 345ºC and 410ºC, respectively. It is apparent that increase in substrate temperature within this range leads to a slight decrease in the average density of InAs islands, owing presumably to the increased surface diffusion of InAs and the associated coarsening. There is indeed a clearly broadening of InAs island size distribution as can be visible by comparing Fig. 17 A, B and C. Calculated values of $\boldsymbol{a_{isl}}$ are plotted as a function of the island base sizes in Fig. 18 A, B and C. Both strained (closed symbols) and relaxed (open symbols) islands are considered. The ratio of relaxed to strained islands increases from 20 to 35% with an increase of substrate temperature from 295ºC to 410ºC. There is a corresponding increase in the average dots size as can be seen from Fig.17 A, B and C. An important feature of Fig.17 is that the size distribution of coherent islands is nearly temperature independent. The substrate temperature increase results primarily in a broadening of the range of island sizes within which coherent and dislocated islands coexist. This range is from 13.7 nm -17.5 nm from samples grown at 295ºC. It increases to from 13.7 nm – 24 nm for samples grown at 410ºC.

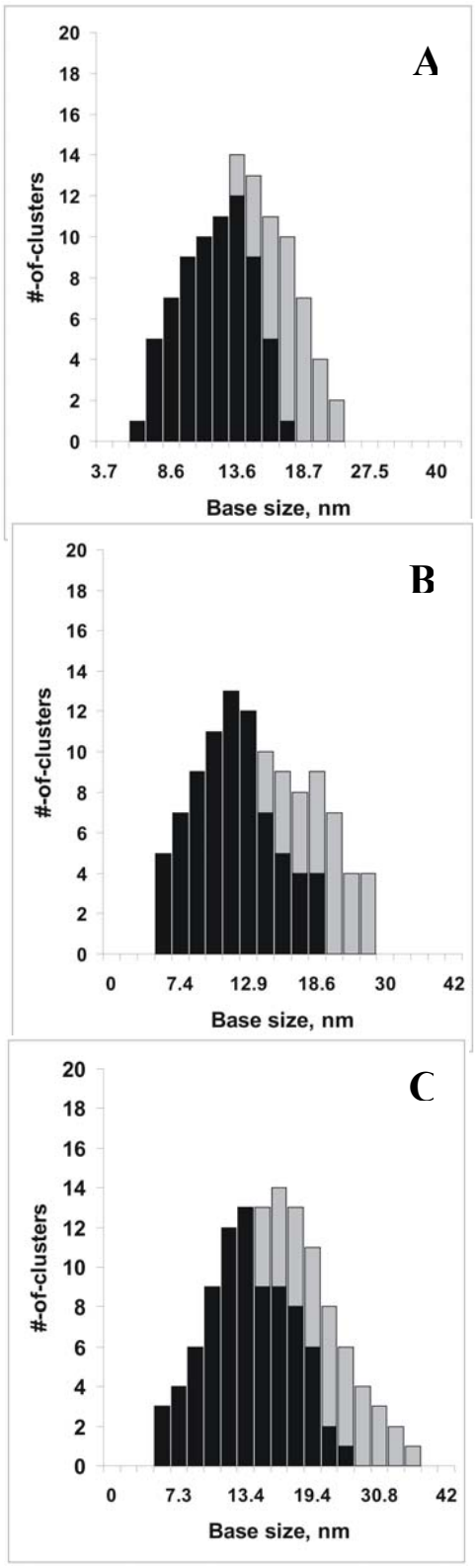

Fig. 17 InAs islands size distribution that corresponds to the same set samples as in Fig.16, showing number of coherent (black) and incoherent (gray) islands as function of their base size.

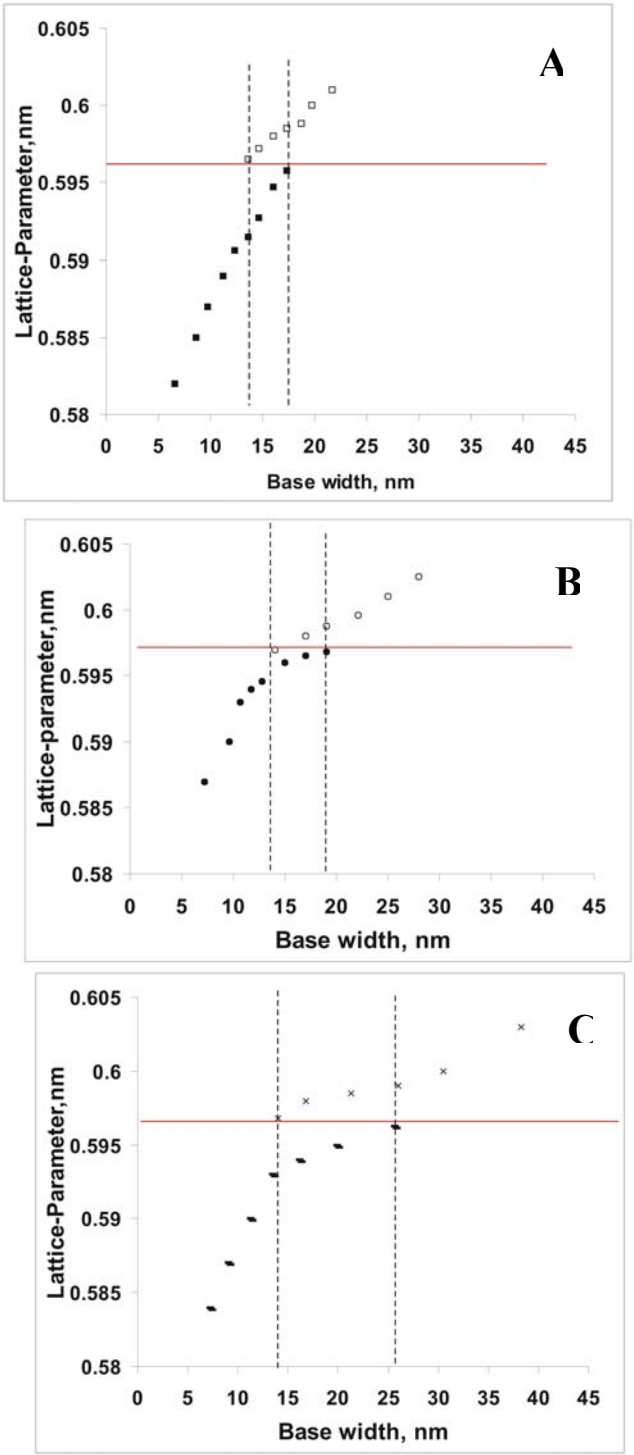

Fig. 18 Plots of an average in plane lattice parameter of InAs islands as a function of their base size for the same set samples as in Fig.16. Horizontal line corresponds to the critical island lattice parameter that indicates the upper limit for the coherent islands. Vertical dashed lines show regions where both coherent and incoherent islands exist.

5) InAs growth on relaxed SiGe buffer layer

InAs dots were grown on relaxed SiGe buffer layer. Fig. 19 shows the typical sample structure. Fig. 20 showed AFM images of Ge dots on relaxed SiGe buffer layer and InAs dots on relaxed

SiGe buffer layer. It is very interesting to notice that InAs dots do not preferentially nucleated over the dislocation network. Comparing to Ge dots on relaxed buffer layers, the growth mode is VW instead of SK and the misfit strain is increased from 4% to 11% for InAs on Si. Which one of these two factors prevents the InAs dots from registering to the underlying dislocation network is an important question to answer. We plan on conducting studies using GaAs on SiGe to single out the chemical incompatibility from the misfit strain in an effort to hunt for the answer to this question.

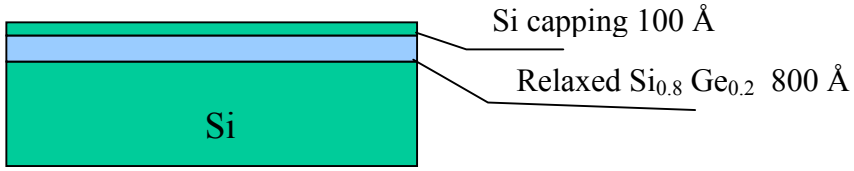

Fig.19, The substrate structure with dislocation network.

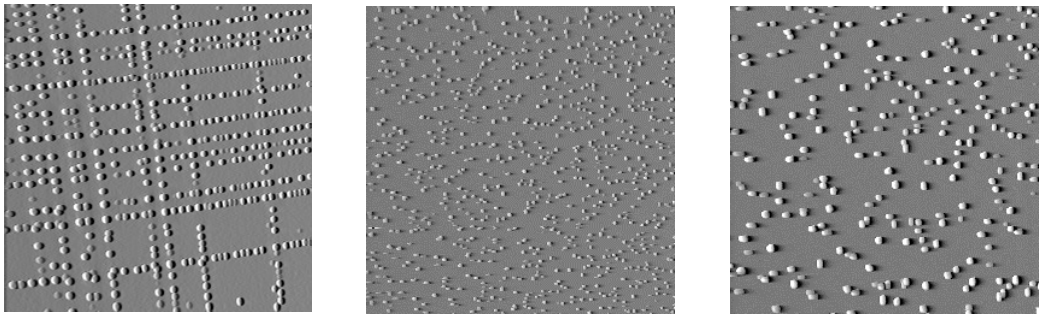

(a) Ge/ Si (b) InAs/ Si (c) InAs/Si

Fig. 20. (a) $5\times5\mu m^2$ AFM image of Ge quantum dots on Si, (b) $5\times5\mu m^2$ AFM image of InAs quantum dots on Si, (c) $3\times3\mu m^2$ AFM image of InAs quantum dots on Si.

6) <u>Contrast between InAs and GaAs on Si (001)</u>

Both InAs and GaAs are grown on Si (001) with the similar growth conditions. A clear difference between the InAs and GaAs growth behavior is the dot density dependence on arsenic BEP. InAs dot density strongly depends on the arsenic BEP, while GaAs dot density is nearly independent on arsenic BEP, as figure 21 shown. This suggests that there is fundamental physical difference between the InAs and GaAs grown on Si (001).

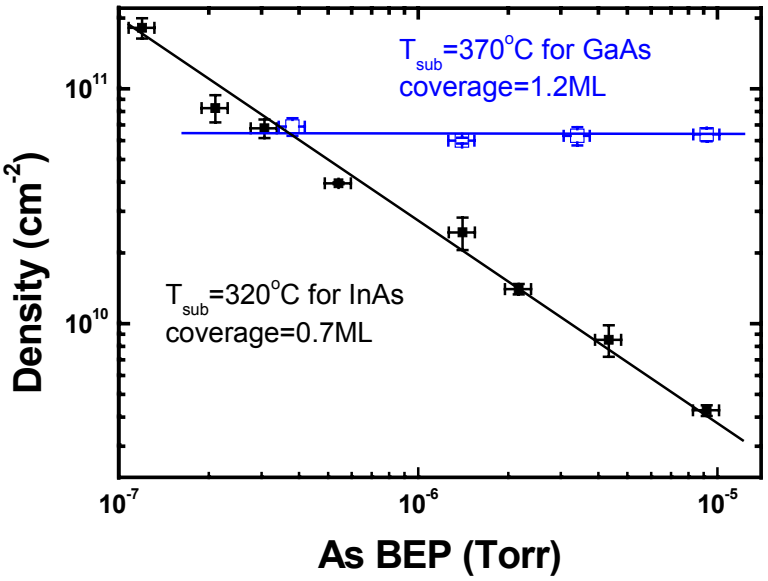

Figure 21. The blue line is the GaAs dot density and black line is the InAs dot density. The growth rate is 0.01 ML/s for GaAs and 0.02 ML/s for InAs. Because the 0.02 ML/s growth rate for GaAs growth is too high to distinguish the dots.

7) <u>High resolution transmission electron microscopy study of InAs on Si (001)</u> :

The detailed structure of InAs on Si(001) is studied via high resolution TEM. The strain is relieved by introducing misfit dislocation at very early growth stages, with island size larger than 4nm, as shown in Fig. 22. Both glissile 60 ^{o} dislocation and sessile 90 ^{o} dislocations are observed by TEM. At the beginning of dislocation formation, the 60 ^{o} dislocation is formed. With increasing size of island, the 90^{o} dislocations appear. It is very likely that the 90^{o} dislocations are formed by two 60^{o} dislocation with increasing dislocation number, as shown in Fig. 23

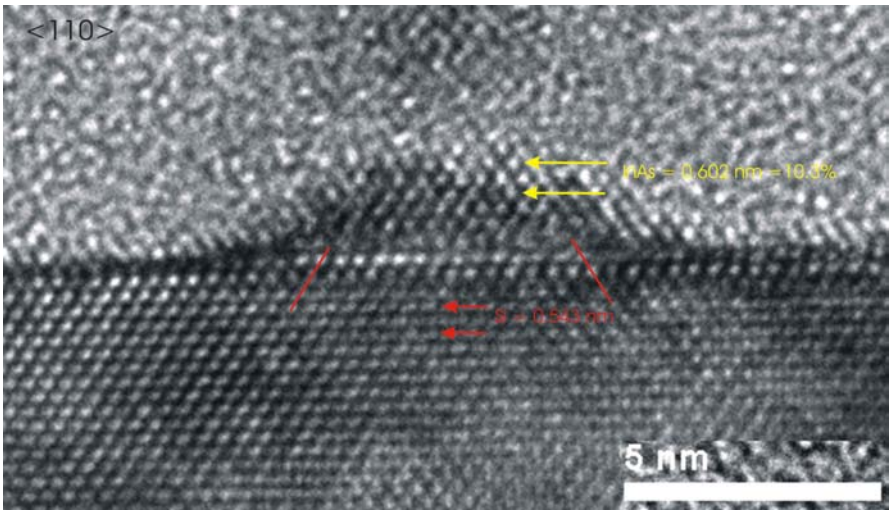

Figure 22. 60^{o} misfit dislocations formed at the interface (indicated by red lines).

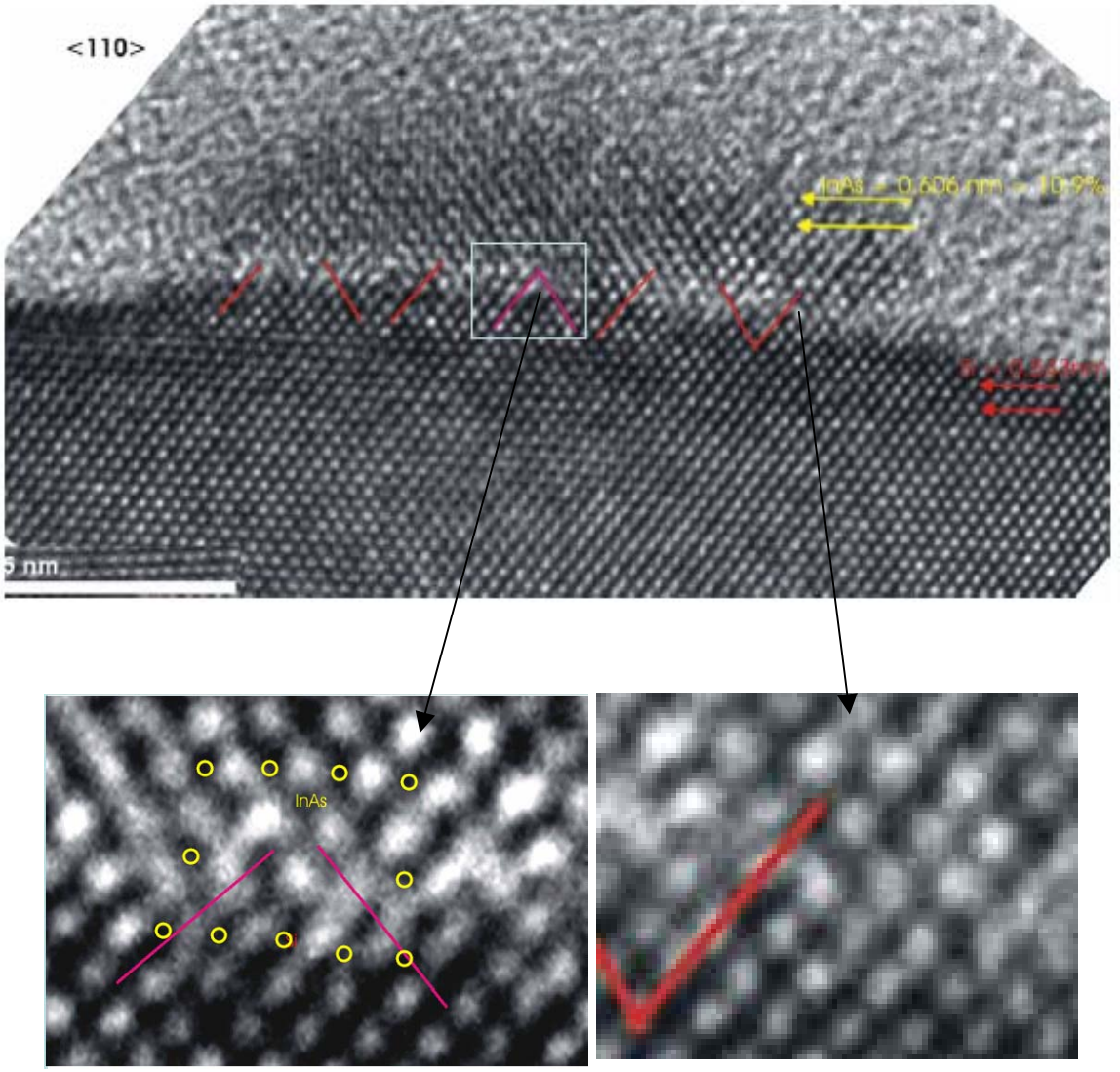

Figure 23. Both 60^{o} and 90^{o} dislocations formed at the interface between Si and InAs. The enlarged images show the detailed atomic structure of dislocations.

8) <u>InAs quantum dots on GaAs</u> :

InAs quantum dots were grown on GaAs using two-step approach. The InAs wetting layer was grown at the 400 ^{o}C and then finished dot growth at 530^{o}C. In this procedure, the high density is improved at the low temperature growth and uniformity is also achieved at high temperature growth. Figure 24 shows the three samples grown a) at low temperature 470 ^{o}C only, b) at high temperature 530 ^{o}C only, and two-step 400 ^{o}C wetting-layer and 530 ^{o}C dot growth.

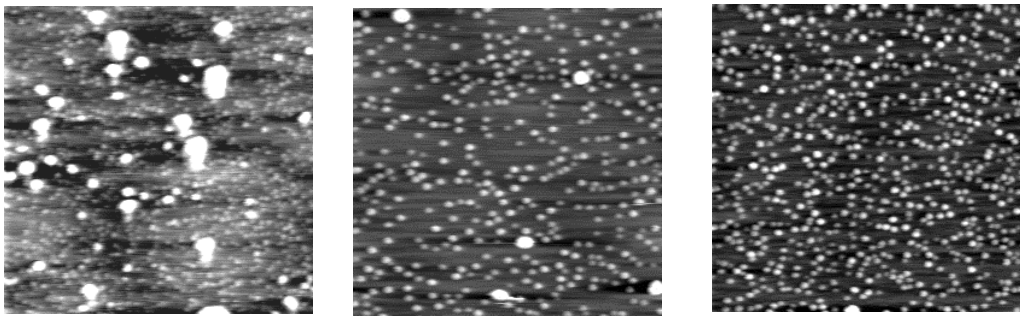

a) b) c)

Figure 24. a) 2.3 ML InAs grown on GaAs (001) at low temperature 470 ^{o}C, b) 2.3 ML InAs grown on GaAs (001) at hihg temperature 530 ^{o}C, c) 1.5 ML InAs grown on GaAs (001) at low temperature 400 ^{o}C and 0.7 ML InAs grown at 530 ^{o}C.

Summary

Tremendous progress is made with regard to the understanding of the self-assembly process via epitaxy in these materials systems during the program of 3+ years. We conducted systematic research into the self-assembly of Ge and III-V quantum dots with lattice mismatch ranging from 4 % (Ge/Si) to 11% (InAs/GaAs) on Si (001) substrates. For material combinations of chemically similar materials, e.g. Ge on Si, or InAs on GaAs, quantum dots growths proceed via Stranski-Krastanow mode. We have demonstrated that buffer layers with a buried misfit dislocation network can be used as an excellent experimental vehicle for the understanding of the quantum dot formation mechanism. Growths on such a buffer layer also gave rise to experimental observations that current understanding could not explain, and deserve further research. We have also studied materials combinations that include both lattice mismatch as well as chemical (or polarity) mismatch. Self-assembly processes behaviors showed new physical phenomenon. We studied the systems with different combinations of chemical and lattice mismatch. Included in the combinations studied are the ones with chemical mismatch only such as GaAs/Ge (001), chemical mismatch with small lattice mismatch such as GaAs/Si (001), and large chemical mismatch with large lattice mismatch such as InAs/Si (001). The systems with chemical mismatch all shows the Volmer-Web growth mode. High resolution TEM indicates that an incoherent interface populated with misfit dislocations between InAs and Si at very early stage of growth. The onset of dislocation as quantum dot sizes as small as 5 nm as observed by our study presents a fundamental barrier to optical device applications such as lasers based on III-V quantum dots on Si (001). All of the conclusions from this project give the fundamental instruction for quantum dots grown and device fabrication,

Publications

"Effects of growth temperature and arsenic pressure on size distribution and density of InAs quantum dots on Si (001)" Z. M. Zhao, O. Hul'ko, H. J. Kim, J. Liu, B. Shi and Y. H. Xie, Thin Solid Film, (to be published)

"Growth and characterization of InAs quantum dots onSi(0 0 1) substrates" Z.M. Zhao, O. Hul'ko, H.J. Kim, J. Liu, T. Sugahari, B. Shi, Y.H. Xie, J. Cryst. Growth, 271, 450 (2004)

"A technique for the measurement of surface diffusion coefficient and activation energy of Ge adatom on Si(001)" H. J. Kim, Z. M. Zhao, J. Liu, V. Ozolins, J. Y. Chang, and Y. H. Xie, J. Appl. Phys. 95, 6065 (2004)

"On the formation mechanism of epitaxial Ge islands on partially relaxed SiGe buffer layers" H. J. Kim, J. Liu, Z. M. Zhao, and Y. H. Xie, J. Vac. Sci. Technol. B 22, 2257 (2004)

"Three-stage Nucleation and Growth of Ge Self-Assembled Quantum Dots Grown on Partially Relaxed SiGe Buffer Layers", H.J. Kim, Z.M. Zhao, and Y.H. Xie, Phys. Rev. B 68, 205312 (2003)

"Influence of a buried misfit dislocation network on the pyramid-to-dome transition size of Ge self-assembled quantum dots on Si(001)," H.J. Kim, J.Y. Chang, and Y.H. Xie, J. Cryst. Growth, Vol. 247, 251 (2003);

"Influence of coupling effect in the operation of vertically coupled quantum dot lasers", Bin Shi and Y.H. Xie, Appl. Phys. Lett. 82, 4788 (2003)

"Influence of the wetting-layer growth kinetics on the size and shape of Ge self-assembled quantum dots on Si(001)," H.J. Kim and Y.H. Xie, Appl. Phys. Lett. **79**, 263 (2001).

Talks

"Three-stage nucleation and growth of Ge self-assembled quantum dots grown on partially relaxed SiGe buffer layers" HyungJun Kim, ZuoMing Zhao, Ya-Hong Xie, Material Research Society Spring Meeting, San Francisco, April 14, 2004

"InAs quantum dots growth on Si (001) substrates" The Workshop on Compound Semiconductor Materials and Devices, Pasadena, Zuoming Zhao Ya-hong Xie, California February 15-18, 2004.

"Understanding the Physics of Self-assembled by Epitaxy of Quantum Dots of Cubic Semiconductors" The 4th International Workshop on Semiconductor Quantum Structures and Nano-Photonics, HyungJun Kim, ZuoMing Zhao, Joon-Yeon Chang, Ya-Hong Xie, Korea, November 26, 2003

" A novel technique for the measurement of ge adatom surface migration length on Si (001)" H. J. Kim, Joon-Yeon Chang, Y. H. Xie, Material Research Society Spring Meeting, San Francisco, April, 2002.

"Fabrication of self-assembled quantum dots in cubic semiconductor materials for device applications", Ya-Hong Xie, presented at the Workshop of the Institute for Pure and Applied Mathematics (IPAM), Lake Arrowhead, CA, December 2002 (invited);

"The influence of a buried misfit dislocation network on the pyramid-to-dome transition size in Ge self-assembled quantum dots on Si(001)", H.J. Kim, J.Y. Chang, and Y.H. Xie, June 22, 2001, Electronic Materials Conference, South Bend, IN;

"Fabrication of Self-assembled Quantum Dots", Y.H. Xie, March 28, 2001, Naval Research Laboratory, Electronics Science and Technology Seminar, Washington DC (INVITED);

People supported by this program (100% and/or partially)

Ya-Hong Xie	PI (partial)
Oksana Hul'ko	Postdoc (partial)
HyungJun Kim	Graduate student (partial)
Jian Liu	Graduate student (partial)
ZuoMing Zhao	Graduate student (partial